MOUNTAIN-PLAINS CONSORTIUM

MPC 24-547 | S. Banerji, Md. A. Al Sarfin, and A.D. Sorensen

DURABILITY AND VOLUMETRIC STABILITY OF NON-PROPRIETARY ULTRA-HIGH-PERFORMANCE CONCRETE MIXES BATCHED WITH LOCALLY SOURCED MATERIALS

MOUNTAIN-PLAINS CONSORTIUM REGION 8

A University Transportation Center sponsored by the U.S. Department of Transportation serving the Mountain-Plains Region. Consortium members:

Colorado State University
North Dakota State University
South Dakota State University
University of Colorado Denver
University of Denver
University of Utah
Utah State University
University of Wyoming

Technical Report Documentation Page

1. Report No.	2. Government Accession No.	3. Recipient's Catalog No.
MPC-695		

4. Title and Subtitle	5. Report Date
Durability and Volumetric Stability of Non-Proprietary Ultra High Performance Concrete Mixes Batched With Locally Sourced Materials	August 2024
	6. Performing Organization Code

7. Author(s)	8. Performing Organization Report No.
Srishti Banerji, Ph.D. Md. Abdullah Al Sarfin, M.S. Andrew D. Sorensen, Ph.D., P.E.	MPC 24-547

9. Performing Organization Name and Address	10. Work Unit No. (TRAIS)
Dept. of Civil & Environmental Engineering Utah State University 4110 Old Main Hill Logan, UT 84322-4110	11. Contract or Grant No.

12. Sponsoring Agency Name and Address	13. Type of Report and Period Covered
Mountain-Plains Consortium North Dakota State University PO Box 6050, Fargo, ND 58108	Final Report
	14. Sponsoring Agency Code

15. Supplementary Notes

Supported by a grant from the US DOT, University Transportation Centers Program

16. Abstract

Ultra-high-performance concrete (UHPC) is distinguished by its superior mechanical and durability properties. These characteristics are attained through a precise mixture design that includes a low water-to-cement ratio, high fineness supplementary cementitious materials (SCMs), and steel fibers. This report presents the evaluation of durability and volume stability properties of a non-proprietary UHPC mixture using locally sourced materials in Utah. This study uses response surface methodology and central composite design to optimize the UHPC mixture. The optimized UHPC mixture with 2% steel fiber by volume achieves 22,113 psi (153 MPa) compressive strength. The freeze-thaw durability test shows minimal degradation, with the retained dynamic modulus of elasticity of over 99.1% after 90 cycles. Compared with similar studies, UHPC specimens are expected to degrade less than the UDOT specified limit of 96% after 600 cycles. The average electrical resistivity of the UHPC specimens is 192 kΩ-cm, which indicates very low chloride-ion penetration. The volume stability test results demonstrate impressive performance as well. The drying and autogenous shrinkage strain of the mixture after 80 days are 365 and 225 microstrain, respectively. Thus, the drying shrinkage strain is about half of the UDOT acceptable limit of 766 microstrain. Overall, the developed locally sourced UHPC mix evaluated in this project exhibits excellent mechanical, durability, and volume stability properties. This research project contributes to improve the accessibility and affordability of the material for the widespread use in infrastructures projects to ensure the longevity and reliability of transportation infrastructure.

17. Key Word	18. Distribution Statement
Ultra-high-performance concrete, durability, volumetric stability, non-proprietary mixture	Public distribution

19. Security Classif. (of this report)	20. Security Classif. (of this page)	21. No. of Pages	22. Price
Unclassified	Unclassified	66	n/a

Durability and Volumetric Stability of Non-Proprietary Ultra-High-Performance Concrete Mixes Batched with Locally Sourced Materials

Srishti Banerji
Assistant Professor
Civil and Environmental Engineering
Utah State University

Md. Abdullah Al Sarfin
Graduate Research Assistant
Civil and Environmental Engineering
Utah State University

Andrew D. Sorensen
Associate Professor
Civil and Environmental Engineering
Utah State University

August 2024

Acknowledgements

The authors thank the Mountain-Plains Consortium (MPC) for funding this research. The work in Chapters 2, 3, and 4 was supported in part by the Utah Department of Transportation (Research Project UT-21.102). The authors also acknowledge the valuable inputs, technical and logistical support from UDOT. The authors gratefully acknowledge the contribution of material providers—Bridgesource, Ash Grove Cement Company, and Master Builders Solutions—for their donations at various stages of the project.

Disclaimer

ABSTRACT

Ultra-high-performance concrete (UHPC) is distinguished by its superior mechanical and durability properties. These characteristics are attained through a precise mixture design that includes a low water-to-cement ratio, high fineness supplementary cementitious materials (SCMs), and steel fibers. This report presents the evaluation of durability and volume stability properties of a non-proprietary UHPC mixture using locally sourced materials in Utah. This study uses response surface methodology and central composite design to optimize the UHPC mixture. The optimized UHPC mixture with 2% steel fiber by volume achieves 22,113 psi (153 MPa) compressive strength. The freeze-thaw durability test shows minimal degradation, with the retained dynamic modulus of elasticity of over 99.1% after 90 cycles. Compared with similar studies, UHPC specimens are expected to degrade less than the UDOT specified limit of 96% after 600 cycles. The average electrical resistivity of the UHPC specimens is 192 kΩ-cm, which indicates very low chloride-ion penetration. The volume stability test results demonstrate impressive performance as well. The drying and autogenous shrinkage strain of the mixture after 80 days are 365 and 225 microstrain, respectively. Thus, the drying shrinkage strain is about half of the UDOT acceptable limit of 766 microstrain. Overall, the developed locally sourced UHPC mix evaluated in this project exhibits excellent mechanical, durability, and volume stability properties. This research project contributes to improve the accessibility and affordability of the material for the widespread use in infrastructures projects to ensure the longevity and reliability of transportation infrastructure.

TABLE OF CONTENTS

LIST OF TABLES

LIST OF FIGURES

EXECUTIVE SUMMARY

This report outlines the development of ultra-high-performance concrete (UHPC) mixtures using locally available materials from Utah. This study develops a first-of-its-kind Utah-based non-proprietary UHPC that is both cost-effective and durable, enhancing the longevity of infrastructure while addressing economic and environmental challenges.

UHPC stands out from traditional concrete due to its superior mechanical and durability properties. The enhanced performance of UHPC includes high compressive strength, tensile strength, post-cracking ductility, and high resistance to chloride ion penetration and freeze-thaw cycles, making it significantly more durable than conventional concrete. Such properties are achieved through meticulous composition design and specialized production techniques. As such, a high performing UHPC mixture requires a precise mix of components. The fundamental concepts of developing UHPC are low water-to-cement ratio, utilization of supplementary cementitious materials (SCM), specialized curing regimes to enhance the pozzolanic reaction, and the inclusion of fibers to improve tensile and post-cracking behavior. Despite the UHPC's excellent properties, the high cost of proprietary mixtures has limited its widespread use in infrastructure projects. This research seeks to develop an economical, non-proprietary UHPC mixture using local materials from Utah, making it more accessible for infrastructural development. The aim of this project is to examine the durability and volume stability of this locally sourced UHPC mix design. These two items are of specific interest to local transportation agencies as the typical UHPC application is for bridge closure pours.

This paper's comprehensive literature review highlights UHPC's history and recent developments, its material composition, mixture design, and curing methods. In this research, Type I/II Portland cement is used. A wide variety of SCM and admixtures were considered for UHPC development. Considering availability and simplicity of the mixture design, silica fume and fly ash are used in this research as SCM. A high-range water reducing admixture and high-quality fine quartz sand is utilized. The existing body of research shows a relatively large dosage range of these mix ingredients with non-linear relationships between the mix proportions and resulting material properties. Therefore, a robust statistical technique, response surface methodology along with central composite design, is employed in this study to optimize the non-proprietary UHPC mixture design.

The optimized UHPC mixture can attain the target characteristic compressive strength and adequate workability. The optimized mixture with 2% steel fibers by volume achieved compressive strength of over 22,113 psi (153 MPa), qualifying as UHPC. The freeze-thaw durability test shows minimal degradation, with the dynamic modulus of elasticity remaining at 99.1% after 90 cycles. The Utah Department of Transportation (UDOT) sets the limit for dynamic modulus of elasticity degradation at 96% after 600 cycles. Although this test is still ongoing due to the associated prolonged testing time, results obtained at this stage show impressive durability of the specimens under rapid freezing and thawing conditions. The average electrical resistivity of the UHPC specimens is 192.58 kΩ-cm, which indicates very low chloride-ion penetration, thus reducing corrosion risk. After 80 days of testing, the drying and autogenous shrinkage strain of UHPC are 365 and 225 microstrain. The maximum long-term shrinkage strain limit of UHPC specified by UDOT is 766 microstrain. Based on the test results, the UHPC mixture demonstrates superior mechanical, durability, and volume stability properties. Therefore, the developed non-proprietary UHPC mixture can be suitable for infrastructure applications in Utah weather.

1. INTRODUCTION

1.1 Background and Motivation

Ultra-high-performance concrete (UHPC) is an advanced class of cementitious material with superior mechanical and durability properties. The production of this material requires careful blending of the selected ingredients, optimization of granular mixtures to enhance the compacted density, low water-to-cement ratio, higher dosages of plasticizer to address loss of flowability associated with such lower water content, a specific curing regime that often involves heat and pressure treatment to enhance the microstructure of the matrix as well as to accelerate the hydration process, addition of fibers to improve the tensile and post-cracking behavior, and other steps. (Reda, Shrive and Gillott, 1999; Graybeal and Hartmann, 2003; Graybeal, 2005; Bajaber and Hakeem, 2021; Du et al., 2021).

Several definitions of UHPC are available—all focusing on the impressive strength of the material. ACI 239R-18 defines UHPC as a cementitious material with a minimum compressive strength of 22,000 psi (150 MPa) with specified durability, tensile ductility, and toughness requirements (ACI 239R, 2018). ASTM C1856 puts a lower minimum limit of 17,000 ksi on UHPC's compressive strength (120 MPa) (ASTM C1856/C1856M, 2017). The Federal Highway Administration (FHWA) has a slightly higher minimum specified compressive strength (17,500 ksi or 120.7 MPa) and a sustained post-cracking tensile strength greater than 0.75 ksi (5 MPa) (FHWA, 2023).

The impressive properties of UHPC promise to extend the lifespan of critical infrastructure and, therefore, reduce the cost of construction, repair, and maintenance over the lifetime of such structures. However, the higher price of proprietary UHPC is often a prohibitive factor. Proprietary UHPC can cost between $1,500 to $3,000 per cubic meter ($1,640 to $3,280 per cubic yard) (Shah, Yuan and Photwichai, 2022), whereas the cost of conventional concrete is less than $131 per cubic meter ($100 per cubic yard) (URMCA, 2024). As such, development of non-proprietary, cost-effective UHPC is at the forefront of recent concrete research.

The motivation of this research centers on the development, optimization, and characterization of non-proprietary UHPC mixtures developed for Utah Department of Transportation (UDOT) by utilizing locally sourced Utah materials. While the proprietary UHPC mixtures have dominated the construction industry, this research is driven by the need to make this material more accessible and affordable for the widespread use in infrastructure projects to ensure the longevity and reliability of Utah infrastructures. Therefore, this research addresses the economic and environmental challenges associated with the high material, construction, and maintenance costs, as well as limited access to UHPC.

In a parallel UDOT-funded research project, the authors developed a first-of-its-kind Utah-based nonproprietary UHPC. This research project focuses on evaluating the volumetric stability and durability properties of the developed UHPC mixture. As part of durability, freeze-thaw resistance, and chloride-ion penetrability—essential for the longevity of the material in Utah environment—are investigated. In addition to these tests, the volumetric stability is quantified by evaluating the drying shrinkage and the autogenous shrinkage tests. Moreover, an extensive literature review to identify the current knowledge and research gaps is presented.

1.2 Objective

The objective of this research project is to determine the durability and volumetric stability of a non-proprietary UHPC mix batched with materials commonly available in the Salt Lake City, Utah, area. The specific properties to evaluate the durability are freeze-thaw and chloride ion penetration. The properties to be assessed for volumetric stability are length change and autogenous shrinkage.

1.3 Outline of the Report

This report is organized into five chapters. The first chapter provides the general background, motivation, and objective of this report. The second chapter is a compilation of the relevant body of research works and historical and recent development of the material. The third chapter covers the theoretical and experimental methodology used to carry out the research presented in this report. The fourth chapter presents the findings of the experimental program, and the optimized non-proprietary mixtures developed for the Utah Department of Transportation, including details on the durability and volumetric stability characteristics of the mixture. The fifth and final chapter consolidates the outcomes and summarizes the key findings.

2. LITERATURE REVIEW

2.1 Introduction

This chapter provides a review of the existing literature on development of ultra-high-performance concrete (UHPC). The review includes the historical and recent developments of the material, the material compositions, mixture design, proprietary and non-proprietary mixtures, curing, and mechanical and durability properties of UHPC.

2.2 Development of UHPC

From the mid to late 20th century, academia and industry felt the necessity to develop the next generation of construction materials. This led to the significant development in the field of concrete research, essential to the development of high-strength cement, better understanding of cementitious matrix, a wide variety of supplementary cementitious materials (SCM), development of chemical admixtures, and development and understanding of fiber reinforcement for different concrete variants. These advances have contributed to the development of ultra-high-performance concrete (UHPC). In the mid-1990s, the first UHPC variant was reported by Richard and Cheyrezy (Richard and Cheyrezy, 1994, 1995). Named as reactive powder concrete (RPC), the novel cementitious material was reported to have over 800 MPa (116,000 psi) strength. This research laid the foundation of the advanced construction material today known as UHPC. The underlying principles for achieving such impressive strength enhancement was removing coarse aggregates from the mixture, optimization of the granular mixtures to increase compacted density, application of confining pressure before and during setting, improvement of microstructures by heat-treatment, improvement of ductility by incorporating steel fibers, and incorporation of steel aggregates.

Realizing the significance of the material composition, proportioning, and meticulous optimization of the granular matrix of UHPC, researchers invested in efforts to improve the particle packing density. In 1994, de Larrard and Sedran proposed two models to predict the packing density of a particle mix and optimized the UHPC mix to produce a fluid mortar with a 236 MPa (34,230 psi) compressive strength (de Larrard and Sedran, 1994). Instead of applying high pressure, they achieved the strength with moderate thermal curing for four days at 90°C (194°F), promising industrial feasibility.

Commercial manufacturers also invested heavily in the early development of UHPC. In the 1990s, Lafarge brought a proprietary version of the material DUCTAL® to the market. This fiber-reinforced UHPC was reported to achieved 200 MPa (29 ksi) compressive strength with heat curing at 90°C (194°F) for three days and steel fiber content up to 6% (Chanvillard et al., 1996). Soon, other proprietary UHPC premixes became available in the market. These premixes reportedly had a compressive strength over 200 MPa (29,000 psi), a bending strength over 50 MPa (7,250 psi), and a Young's modulus over 50 GPa (7,250 ksi) (Acker and Behloul, 2004; Maeder et al., 2004; Rossi et al., 2005). However, the high cost associated with the commercial variants of the material has always been prohibitive to the widespread use of UHPC.

In conjunction with the development of the material in the laboratory, extensive research works were carried out to facilitate UHPC's practical application and standardization. In 2002, Association Française de Génie Civil (AFGC) developed the first design guidelines (AFGC, 2002). This document provided recommendations on UHPC's behavior and mechanical characteristics, structural design methods, and durability properties. In 2010, the International Federation for Structural Concrete (fib) also introduced recommendations that apply to high-performance and ultra-high-performance concrete (fib, 2010). The ACI 239R-18 provides guidelines and recommendations for production, properties, design principles, and example applications of UHPC (ACI 239R, 2018). ASTM C1856 specification provides a standard for

UHPC fabrication and testing (ASTM C1856/C1856M, 2017). The Federal Highway Administration (FHWA) has published several documents on the topic of structural design, construction, bridge preservation and repair with UHPC (Haber et al., 2022; Graybeal and El-Helou, 2023).

2.3 Material Composition

UHPC's superior performance is attributed to the meticulously designed material composition, tailored to achieve enhanced mechanical and durability properties. At its core, UHPC components are not that different from the components of ordinary and high-strength concrete. These constituent ingredients are cement, SCMs such as silica fume and fly ash, fine aggregates, water, high range water reducing admixtures (HRWR) or superplasticizers, and fibers. Although coarse aggregates are typically excluded from UHPC, some variants with coarse aggregates are also reported (Wang et al., 2012; Arora et al., 2019; Kodur, Banerji and Solhmirzaei, 2020; Banerji and Kodur, 2022). This section provides a description of the materials used in production and their contribution to UHPC properties.

2.3.1 Cement

Similar to the other concrete variants, the main binder of UHPC is cement. Compared with conventional and high-performance concrete, UHPC utilizes a higher dosage of cementitious materials (Imam et al., 2022). Researchers have investigated the effects of different types of cement on the fresh and hardened properties of UHPC. Dils et al. investigated six different types of cement. These were selected based on their low tricalcium aluminate (C_3A) content and moderate Blaine-fineness. They concluded that cement with a low C_3A specific surface, adequate C_3A/SO_4^2 ratio, and alkali content is preferred (Dils, Boel and De Schutter, 2013). Wille et al. reported that the most preferable UHPC types in the U.S. are Type I Portland cements with low C_3A and low-to-moderate fineness (Wille, Naaman, and Parra-Montesinos, 2011). Other researchers also reported that the cement containing low to no C_3A is preferred since such cement reduces water demand (de Larrard and Sedran, 1994; Collepardi et al., 1997). Type II/V cements are also found to be suitable for the compressive strength and workability of UHPC (Wille, Naaman and Parra-Montesinos, 2011). Alkaysi et al. investigated UHPC produced with Portland Type I/GGBS, Portland Type V, and white cement and reported that the type of cement affects the porosity of the material. Portland Type I/GGBS cement blend resulted in the least permeable product (Alkaysi et al., 2016). Shahrokhinasab et al. investigated the effects of five different cements (Shahrokhinasab et al., 2021). These cements differed by type and manufacturer. They reported that UHPC with masonry cement developed the least compressive strength and density, possibly due to increased lime content. Type III cement resulted in the highest compressive strength as well as reduced working time. The compressive strength of UHPC produced with Type I/II and Lehigh White cement were lower than the compressive strength of UHPC with Type III cement. Based on their study, they recommended Type I/II cement as it led to reasonable strength, consistency, and working time. Microfine cements and superfine cements are also used to improve the packing density of the matrix and thus enhance UHPC properties (Strunge and Deuse, 2008; Xiao, Deng, and Shen, 2014). Researchers have also reported a significant amount of unhydrated cement in hardened UHPC due to insufficient water and/or space. This unhydrated cement works as an expensive filler in the binder system. The amount of unhydrated cement can be reduced by using cement substitutions such as limestone powder (Huang et al., 2017). While this unhydrated cement imparts some self-healing potential to the hardened product under cracking conditions, it also warrants extensive study on UHPC volume stability in moist environments (Wang et al., 2015).

Manufacturing cement is energy intensive and has significant environmental effects. Cement production is the third largest source of anthropogenic carbon emission (Andrew, 2018). Therefore, one of the recent UHPC research trends is focused on producing eco-friendly UHPC with efficient use of cement and other UHPC components (Yu, PHJH Spiesz, and Brouwers, 2015; Amran et al., 2023).

2.3.2 Silica Fume

Silica fume is the most commonly used SCM in UHPC production. The effect of silica fume in concrete technology is well studied. Silica fume concrete has been reported to demonstrate superior performance in terms of compressive strength, tensile strength, flexural strength, elastic modulus, toughness, and steel-concrete bond (Khedr and Abou-Zeid, 1994; Mazloom, Ramezanianpour, and Brooks, 2004; Bhanja and Sengupta, 2005; Nochaiya, Wongkeo, and Chaipanich, 2010).

Silica fume addition in UHPC can have two positive effects: high silica fume content increases compressive strength aided by pozzolanic effects through different curing techniques (Toutanji and Bayasi, 1999), whereas its low density reduces the specific weight of the final product. The resulting low specific weight can result in substantial weight saving (Sadrekarimi, 2004).

UHPC strength improvement with and without fibers by adding up to 20% silica fume is reported by Wu et al. (Wu, Khayat, and Shi, 2019). They also reported that, due to increased viscosity and air entrapment, the strength is decreased by 8% at a silica fume dosage of 25%. As such, they concluded that the optimum dosage for silica fume to maximize the compressive strength is 10% to 20%. They also found that at 10% to 15% silica fume content, the UHPC tensile and flexural behavior is enhanced. With 2% straight steel fibers by volume, they reported 17.2 MPa (2,500 psi) tensile strength and 7.84 MPa (1,137 psi) flexural strength with 10% and 15% silica fume content, respectively.

Xu et al. reported that the addition of silica fume along with thermal curing can positively influence the hydration process and pore structure of UHPC (Xu et al., 2023). The pozzolanic reaction of silica fume is less active at lower temperatures. However, curing at a high temperature can significantly enhance the pozzolanic reaction. As the thermal curing is accelerated by elevated temperature, the compressive strength and pore structure of the hardened matrix also improves. They reported that the optimal dosage of silica fume is 20%. Beyond this limit, the hydration process is hindered due to increased viscosity.

Xi et al. reported that by providing extra nucleation sites for hydration products, silica fume significantly impacts the early age hydration (within first three days) (Xi et al., 2022). This is because of the larger specific surface and presence of silanol groups on the surface. The silanol groups react with calcium hydroxide in the alkaline pore solution. This promotes the adsorption of Ca^{2+} ions and increases the dissolution rate of silicate phases. Furthermore, silica fume competes with cement particles for the adsorption of polycarboxylate ether based superplasticizers. This partially hinders the retarding effect of such superplasticizers on hydration. As a result, UHPC paste with silica fume has enhanced early hydration and shorter induction period. UHPC strength development in later days is attributed to the pozzolanic reaction of silica fume.

The fineness of silica fume particles increases the water demand and reduces the setting time and workability (Nochaiya, Wongkeo, and Chaipanich, 2010). High fineness of silica fume can also increase the viscosity of fresh UHPC (Ma et al., 2004a). Silica fume alters the rheology of the mix. At higher content, it reduces shear-thickening by decreasing particle friction (Wu, Khayat, and Shi, 2019). They also reported that the HRWR demand in UHPC initially decreases as silica fume is added. However, at higher silica fume dosage, the HRWR demand increases. The fluidity enhancement of the mixture at lower silica fume content is attributed to its ability to fill gaps between particles; whereas the increased HRWR demand at higher dosage is attributed to the increased surface area of the fine silica fume particles. Lin et al. investigated the “ball effect” and “plasticizing effect” to explain the influence of silica fume on UHPC fluidity (Lin et al., 2019). In the UHPC mixture, part of the water fills the space between solid particles and part of the water covers the surface of the particles. The filling water has little effect on the mixture’s fluidity. Part of the surface water is absorbed on the particle surface and the rest creates a film on the outside surface. The researchers explained that, under a natural state, the silica fume and

cement particles agglomerate to a flocculant structure, which restrains plenty of free water and reduces fluidity. However, the particle surfaces can be filled with a layer of active material by means of force mixing and adding superplasticizers. Thus, electrostatic repulsion among particles is developed and the flocculent structure is broken. At this stage, the silica fume particles, resembling a "ball" fill in the void of the cement particles, allows the cement particles to slide. This action is defined as the ball effect. Additionally, the voids among the cement particles can be filled by smaller silica fume, and the filling water is replaced to thicken the water film layer of the particles. This is defined as the plasticizing effect. By means of these two effects, the UHPC mixture fluidity increased.

UHPC fiber pullout behavior is influenced by the addition and dosage of silica fume. Wu et al. reported that at 10% to 20% silica fume dosage, the fiber-matrix bond strength increases by 5.5 times compared with the reference mixture (Wu, Khayat, and Shi, 2019). However, a significant reduction of bond strength is reported at 25% dosage of silica fume. Another research reported that at 20%–30% silica fume-cement ratio, the bond strength and the fiber pullout energy are maximum in RPC (Chan and Chu, 2004). The enhancement is more pronounced for the pullout energy. At higher silica fume content, a large amount of hardened cementitious materials adheres to the fiber surface, resulting in the improvement of pullout energy.

2.3.3 Fly Ash

Fly ash is another common supplementary cementitious material used in UHPC production. A byproduct of the combustion of pulverized coal in electric powerplants, fly ash has been widely used in conventional concrete mainly due to its pozzolanic properties. Note that fly ash and other SCMs are generally used in UHPC production along with silica fume. Kwan and Li reported that the addition of fly ash microsphere increased the packing density and water film thickness of mortar mix, thus improving the flowability and allowing for a reduced water-to-cement ratio (Kwan and Li, 2013). Bahedh and Jaafar reported that the workability of UHPC mixtures increased from 50 mm to 240 mm as the fly ash dosage was increased from 0 to 40%(Bahedh and Jaafar, 2018). Ahmed et al. reported an eco-friendly UHPC with high volume of class F fly ash (Ahmed et al., 2021). They reported that the slump flow of ECO-UHPC increased with the fly ash-to-cement ratio, highlighting the ball bearing effect of spherical fly ash particles in friction reduction.

Dong et al. investigated the compressive strength development of UHPC with high volume fly ash under normal and heat curing conditions (Dong et al., 2020). They varied the fly ash content from 0% to 70%. Under normal curing conditions, their results demonstrated that the early age strength of UHPC decreased as the fly ash content increased. At a later age, maximum compressive strength was achieved with fly ash content between 20% to 30%. They noted that the compressive strength improvement at later ages of UHPC with 70% fly ash was more pronounced compared with the UHPC with 20% to 50% fly ash content. They noted similar trends with heat curing conditions. However, the strength development at early ages for heat treated specimens was faster compared with the specimens with normal curing. Bahedh and Jaafar demonstrated enhanced compressive strength over all ages with 10% to 20% fly ash content (Bahedh and Jaafar, 2018). The densification of the pore structure by incorporating fly ash was attributed to this phenomenon. Ahmed et al. reported that while the addition of class F fly ash generally reduces UHPC compressive strength, ultra-high strength can still be achieved with 40% replacement of Portland cement by fly ash (Ahmed et al., 2021). They also reported a statistically significant decrease in elastic modulus, splitting tensile and flexural strength with increased fly ash content. However, the addition of fly ash reduced the CO_2-footprint up to 58.3%. According to Chen et al., it is possible to increase both compressive and flexural strength with the addition of 10% to 30% fly ash and applying either standard or suitable autoclave curing (Chen, Gao, and Ren, 2018). However, higher fly ash content required higher pressure of autoclave curing.

Bahedh and Jaafar demonstrated a direct relationship between fly ash content and the depth of water permeability in the concrete samples (Bahedh and Jaafar, 2018). As the fly ash content increases, the depth of water permeability decreases. The sample with 40% fly ash content achieved the lowest permeability. The addition of fly ash and increased duration of autoclave curing can reduce UHPC porosity (Chen, Gao and Ren, 2018).

2.3.4 Other Supplementary Cementitious Materials

Apart from silica fume and fly ash, a wide variety of supplementary cementitious materials are used in UHPC production such as slag, limestone powder, metakaolin, quartz flour, nano-silica, and rice husk (Park et al., 2021). Researchers have investigated the contribution of these SCMs to the properties of UHPC. Some of the research efforts are summarized as follows:

- Ha et al. replaced 30% of the ordinary Portland cement (OPC) with grounded blast furnace slag (GBFS) or a combination of grounded blast furnace slag and rice husk ash (RHA) (San Ha et al., 2022). They achieved 151.3 MPa (21.95 ksi) compressive strength for UHPC mixture with 30% GGFS replacement. With 15% GBFS and 15% RHA, the compressive strength was reported to be 143.5 MPa (20.8 ksi). Their work demonstrated that the UHPC mixtures with GGFS and RHA had a lower embedded CO2 emission index compared with the mixtures without these two SCMs. Thus, incorporating GBFS and RHA showed promise to produce UHPC with less environmental impact without compromising the strength. Yalçınkaya and Çopurŏglu reported that ground granulated blast furnace slag (GGBS) replacement significantly reduced the superplasticizer requirement (Yalçınkaya and Çopuroğlu, 2021). They reported achieving almost similar UHPC strength with GGBS to that of without GGBS. However, the difference can be eliminated by addition of fiber and prolonged curing. Yang et al. reported a 17% increase in UHPC setting time with a 50% replacement of cement with phosphorus slag (PS) (Yang et al., 2019). With the addition of PS below 40% replacement level, the compressive strength is negatively affected. However, it can promote long-term strength development. At 50% replacement of cement by PS, the UHPC strength was reported to be lower than the reference sample. PS replacement was found to be beneficial to autogenous shrinkage. By facilitating particle movement, slag cement was reported to improve flowability of UHPC mixtures (Liu et al., 2018). In the early ages, slag cement retards the hydration of the system. At later ages, secondary pozzolanic reaction improves compressive strength. However, slag cement can exacerbate autogenous shrinkage strain due to refined pore structure and the enhanced depletion of moisture.

- Mo et al. reported that the addition of metakaolin up to 15% in UHPC mixtures under various curing conditions improves compressive strength (Mo, Gao, and Su, 2021). However, no compressive strength gain was reported with 20% replacement. Steam curing can be employed to achieve the strength of water cured strength at 90 days for metakaolin-replaced mixtures, signifying the benefit of steam curing for metakaolin-blended UHPC mixtures. In another paper, they reported that, although metakaolin reduced the one-day compressive strength of UHPC mortars, blends with 5% to 20% metakaolin exhibited higher 14-day compressive and flexural strength compared with the control mix (Mo, Wang, and Gao, 2020). Tafraoui et al. reported that equivalent mechanical performance can be achieved by weight for weight substitution of silica fume by metakaolin with a slightly increased mixing time (Tafraoui et al., 2009). Improvement of flexural and mechanical strength through heat curing and steel fibers were reported to be more pronounced with metakaolin-blended mixtures compared with silica fume-blended mixtures. Norhasri et al. investigated the role of nano metakaolin as an additive in UHPC (Norhasri et al., 2016). They reported reduced workability and stronger late effects on the compressive strength. The calcium silicate hydrate (C-S-H) crystals of nano metakaolin were reported to be different compared with the C-S-H crystals in UHPC with OPC and OPC-metakaolin blended samples.

- In a paper by Li et al., limestone powder is reported to improve the workability of UHPC by reducing friction between particles (P. P. Li et al., 2020). This is attributed to the increasing inter-particle electrostatic repulsion due to OH^- groups' localization over the Ca2+ surface, and lowering adsorption and consumption of polycarboxylic ether molecules of superplasticizers. They found that the dilution effect of limestone powder reduced the total amount of hydration products. However, the secondary pozzolanic hydration was reported to be more intensive and thus advantageous to the later-age strength development. Moreover, they concluded that replacing binders with limestone powder can benefit the development of eco-friendly and low-cost UHPC. Other researchers have also demonstrated that replacement of cement with limestone will improve hydration and microstructural development (Huang et al., 2017).

- Nano-CaCO3 can significantly enhance the interfacial bond properties between embedded fiber and UHPC matrix. Wu et al. reported that the compressive and flexural strength of UHPC made with 3.2% nano-CaCO3 reached the maximum. However, excessive dosage of these particles has a negative effect on compressive strength (Camiletti, Soliman, and Nehdi, 2013; Wu, Shi, and Khayat, 2018). Nano-CaCO3 is shown to have a positive effect on workability and early age setting and hardening, as well as comparable or better early age strength compared with the control samples (Camiletti, Soliman, and Nehdi, 2013).

- Yu et al. reported that, at optimum dosage (3.74% by the mass of the binder amount), nano-silica corresponds to the highest UHPC mechanical properties (Yu, Spiesz and Brouwers, 2014). The addition of nano-silica can significantly compensate for the retardation effect of a large superplasticizer dosage. They also reported that due to the nucleation effect of nano-silica, the hydration reaction can be promoted, resulting in more C-S-H gel production. Adding nano-silica delays steel rebar corrosion and extends the service life of structures (Ghafari et al., 2015).

2.3.5 Aggregates

As discussed in section 2.2, a basic principle of UHPC production is the removal of coarse aggregates to improve the homogeneity of the matrix (Richard and Cheyrezy, 1995). Generally, aggregate is the least expensive component of concrete. Aggregate type, shape, texture, and strength are known to affect UHPC properties. Finely ground quartz sand is the most common aggregate used in UHPC production. The particle size of the quartz sand usually varies between 150 μm and 600 μm (Du et al., 2021). However, the cost and availability of high-quality quartz sand is often prohibitive. Therefore, researchers have developed UHPC using a less expensive substitute of high-quality quartz sand. Meng et al. used Missouri river sand (maximum particle size of 4.75 mm [3/16 inch]) and masonry sand (maximum particle size of 2.0 mm [1/16 inch]) (Meng, Valipour, and Khayat, 2017). They reported that a combination of 70% river sand and 30% masonry sand achieved the target PSD using a modified Anderson-Andreasen packing model. Du et al. commented that the large particle size of river and masonry sand leads to a weaker interfacial transition zone (IZT) (Du et al., 2021). As such, optimization of particle packing is necessary to minimize the IZT. Replacing river sand with recycled fine aggregates has also been reported to increase the IZT size and thus have a negative effect on the mechanical properties and flow (Zhang et al., 2018a). Aydin et al. produced very high compressive strength RPC (above 180 MPa or 26.1 ksi) with korund, basalt, limestone, granite, and sintered bauxite aggregates (Aydin et al., 2010). When they evaluated the surface characteristics of the aggregates, they observed high angularity in korund, basalt, and granite. Limestone, which has low strength but rough surface, can be used to produce high strength RPC. The same is true for granite aggregates, which, contrary to limestone aggregates, have smooth surfaces but high strength. They reported relatively lower compressive strength for quartz aggregated RPC (170 MPa or 24.6 ksi). Quartz has a very smooth surface. Liu et al. reported that calcined bauxite aggregate can be used to replace sand in a UHPC mixture (Liu and Wei, 2021). The porous structure in

calcined bauxite aggregates helps to maintain internal relative humidity and works as an internal curing agent. As a result, these aggregates help to reduce autogenous shrinkage.

From its inception, most of the UHPC variants have been developed by discarding coarse aggregates in favor of achieving a homogenous matrix. However, the benefits of coarse aggregates have been noticed by researchers. As such, variants of UHPC with coarse aggregates are reported in the scientific literature (Ma et al., 2004b; Liu et al., 2016; Banerji, Kodur, and Solhmirzaei, 2020; Kodur, Banerji, and Solhmirzaei, 2020; Banerji and Kodur, 2022). Liu et al. replaced fine aggregates with coarse aggregates up to 25% without significantly compromising the first crack strength and fiber bridging stress (Liu et al., 2016). Arora et al. produced UHPC with a combination of coarse and fine aggregate (Arora et al., 2019). The aggregate combination was optimized using a compressible packing model. The compressive and flexural strength of such UHPC was reported to be 150 MPa (21.75 ksi) and 10 MPa (1.45 ksi), respectively. They also observed significant improvement of moisture resistance and ionic transport. Li et al. observed a decrease in compressive and tensile strength of 9.1% and 16.3% after incorporating coarse basalt aggregate (Li, Yu, and Brouwers, 2018). Coarse aggregate can have a positive effect on mixing time and UHPC shrinkage properties. Although UHPC mechanical properties with the addition of coarse aggregate are compromised to some extent, the cost and shrinkage behavior indicates promise for such variants of the material.

2.3.6 Admixtures

One of the major driving forces behind the development of new generation high-strength concrete is the innovation behind chemical admixtures development. The development of a high-range water reducer (HRWR) allows for lower water-to-cement ratio without compromising the fresh properties, i.e., workability, of such mixtures. The most common HRWR used in UHPC production is the polycarboxylate ether (PCE) based superplasticizers. A high dosage of HRWR admixtures tend to prolong the setting time and negatively impact the strength at an early age of UHPC (Li et al., 2016; Du et al., 2021). Li et al. observed a saturation dosage of such admixture beyond which no additional dispersion improvement occurs (Li et al., 2016). The dispersion ability of PCE-based superplasticizers depends on the chemical structure and the ability to adsorb onto particle surfaces. They also noted the delaying effect on setting time of adsorbed and free PCE molecules in an aqueous phase, especially in the first three days. They also reported that the type and dosage of PCE-based superplasticizers affect the absolute chemical shrinkage of paste on the first day and greatly affect the mixture's autogenous shrinkage.

Researchers also reported the use of viscosity modifying admixtures, shrinkage reducing admixtures (SRA), and expansive agents (EA) in UHPC (Du et al., 2021). Cui et al. investigated the effect of three types of viscosity enhancing agents (VEA) on the properties of sprayable UHPC (Cui et al., 2022). These are hydroxypropyl methyl cellulose (HPMC), polyacrylic acid, and welan gum. They reported that HPMC is the most suitable agent for sprayable UHPC. All three types of VEA improved the yield stress and plastic viscosity of the mixture. Teng et al. reported that shrinkage reducing admixtures with lightweight sand is effective to lower autogenous shrinkage without compromising mechanical properties (Teng, Addai-Nimoh, and Khayat, 2023). They also noted that lightweight sand counteracts the negative effect of SRA on hydration and pozzolanic reaction of silica fume. Autogenous shrinkage can also be reduced by calcium-sulfoaluminates-CaO-based EA. However, the early-age autogenous shrinkage reduction with EA is limited. Besides, the risk of cracking is reported to be very high when the EA dosage reaches 15% of the binder content (Shen et al., 2020).

2.3.7 Fibers

Fiber plays a significant role in compressive, tensile, flexural properties of UHPC as well as achieving ductility and toughness. A wide variety of fibers are used in UHPC production. The common types of fibers used in UHPC are steel fibers, polyvinyl alcohol (PVA) fibers, carbon fibers, polypropylene (PP) fibers, and glass fibers. Meng and Khayat investigated the effects of hybrid fibers on fresh, mechanical, and shrinkage properties of cost-effective UHPC (Meng and Khayat, 2018). On the fresh properties of the mixtures, they reported decreased workability of the mixtures as the steel fiber content increased from 0% to 5%. For an increase of fiber volume fraction from 2% to 5%, the HRWR demand increased threefold to maintain the workability. At 2% fiber content, the HRWR demand increased 25%; when 0.5%, straight steel fibers were replaced by PVA fibers. On the flexural strength, they reported 23 MPa (3,336 psi) strength with 4% straight steel fiber content. However, the flexural strength of the specimens decreased as the fiber content exceeded the critical value (2% or 4%). This was attributed to the agglomeration of fibers. With 5% straight fibers by volume, 60% reduction of autogenous shrinkage was observed (Meng and Khayat, 2018). Akça and Ipek discussed UHPC mixtures with short straight steel fibers (l = 6 mm, d = 0.2 mm) and long hooked-end steel fibers (l = 35 mm, d = 0.75 mm) (Akça and Ipek, 2022). They reported that compared with mixes with 2% short steel fibers, mixes with 3% hybrid fiber (combination of straight and hooked-end fibers) increased the compressive and flexural strength by 16% and 48%.

Huang et al. demonstrated that 20-mm long steel fibers improve the pullout load and energy by 5- and 27-fold, respectively, compared with 6-mm long steel fibers and thus significantly increased flexural strength and toughness (Huang et al., 2021). They implemented a flow-induced casting device to achieve preferred fiber orientation. This resulted in a 75% improvement in flexural strength and 100% improvement in toughness compared with randomly oriented fibers. Orgrass and Klug reported that combining short, high-strength steel fibers with long normal strength steel fibers can improve the post-fracture behavior of UHPC (Orgass and Klug, 2004). They also described the brittle behavior of UHPC with 1% fiber by volume where the failure is controlled by a single vertical crack. On the other hand, at the 2% fiber volume fraction, the failure is controlled by a single main vertical crack accompanied by multiple smaller cracks. Yao et al. demonstrated that with PVA fiber, a low volume fraction (0.5%) or longer fibers (12 mm) significantly inhibited shrinkage deformation (Yao et al., 2024). The mechanical strength of the mixtures also peaked for a 0.5% fiber volume fraction. Based on these two observations, they concluded that optimum fiber volume fraction and length for PVA fibers are 0.5% and 12 mm, respectively. Dehghanpour et al. reported a comprehensive study with varying fiber volumes of PVA, glass, and steel fibers (Dehghanpour et al., 2022). They reported that steel fibers demonstrated exceptional positive effects on UHPC's mechanical properties. The dynamic test revealed that the UHPC damping ratio increases with the increase in fiber ratio regardless of fiber type. He et al. compared the mechanical properties of UHPC reinforced with glass fibers and high-performance polypropylene fibers (He et al., 2021). They concluded that the optimum dosage of fiber is 2%. Their research suggests that the mechanical properties of UHPC do not necessarily improve with increased fiber content. They also reported higher compressive and flexural strength with glass fibers compared with high-performance polypropylene fibers. Banerji et al. demonstrated that polypropylene fibers significantly enhance the fire resistance of UHPC beams by reducing the extent of fire induced spalling (Banerji, Kodur, and Solhmirzaei, 2020). Recycled carbon fibers have comparable positive effects on the tensile and compressive strength of UHPC to steel fibers (Patchen, Young, and Penumadu, 2022).

2.4 Mixture Design

As discussed earlier, the principle of achieving the superior material properties of UHPC depends on achieving dense and improved microstructure of the matrix. Researchers have investigated different mix design techniques. These techniques include packing model, statistical mixture design, methods based on rheological properties of paste, and machine learning-based models (Zhou et al., 2021).

Primarily, the packing models used in UHPC mixture design can be classified as dry and wet packing density models. Dry packing density refers to the proportion of solid volume to the total volume of systems. The dry packing models are classified as discrete and continuous packing models. As the name suggests, discrete packing models are based on the assumption of particle sets with a specific size. On the other hand, continuous packing models consider the continuity in particle size. Continuous packing models are more suitable for UHPC mixture design as they achieve higher packing density (Dingqiang et al., 2020; Du et al., 2021; Zhou et al., 2021).

Among the dry continuous particle packing models, the Modified Andersen & Andreasen (MAA) particle packing model is the most popular one (Funk and Dinger, 2013). The MAA packing model provides a target particle distribution curve, as shown in (Eq. 1).

$$P(D) = \frac{d^q - d_{min}^q}{d_{max}^q - d_{min}^q} \times 100 \quad \text{(Eq. 1)}$$

Where, $P(D)$ = cumulative percent finer than size d
D = size of the particle
d_{min} = minimum particle size
d_{max} = maximum particle size
q = distribution modulus

The distribution modulus q in the equation determines the ratio of fine to coarse particles. For UHPC, Yu et al. developed an eco-friendly UHPC mixture using q = 0.23 (Yu, Spiesz, and Brouwers, 2015). However, Wang et al. demonstrated that this value of the distribution modulus may not always guarantee the densest particle packing (Wang et al., 2022). They reported maximum compressive strength with q ranging from 0.17 to 0.19. The mixture proportion can be adjusted by using an optimization algorithm such as least square method (LSM) as shown in (Eq. 2).

$$RSS = \sum_{i=1}^{n} \left(P_m\left(D_i^{i+1}\right) - P_{tar}\left(D_i^{i+1}\right) \right)^2 \quad \text{(Eq. 2)}$$

Where, P_{mix} = Composed mixed
P_{tar} = Target grading from (Eq. 2)

Researchers have noted that the dry packing models fail to capture the contribution of liquids such as water and admixtures. For example, Wang et al. demonstrated that, among all raw materials, superplasticizer has the most significant effect on the mixture's packing density (Wang et al., 2019). As such, the wet packing density model is proposed to quantify the contribution of liquid components of the mixture to packing density (Wong and Kwan, 2008). In this method, after setting an initial water-to-binder ratio and preparing the mixture, the paste is transferred to a cylindrical mold of known volume. At this stage, if required, appropriate compaction is applied. Then the solid concentration or packing density (ϕ) and void ratio (u) are calculated using (Eq. 3). Next, the water-to-binder ratio is lowered and the whole process is repeated until the maximum packing density is achieved.

$$V_c = \frac{M}{\rho_w u_w + \rho_\alpha R_\alpha + \rho_\beta R_\beta + \rho_\gamma R_\gamma}$$

$$u = \frac{V - V_c}{V_c}$$

$$\phi = \frac{V_c}{V} \quad \text{(Eq. 3)}$$

Where, ρ_w = Density of water
ρ_α, ρ_β, and ρ_γ = Solid densities of α, β, and γ
R_α, R_β, and R_γ = Volumetric ratio of α,β, and γ
V_c= Solid volume of cementitious materials
V, M = Volume and mass of the paste in the mold, respectively.

The higher number of ingredients and the relatively wide range of their dosage in UHPC leads to complexity in mixture design. Moreover, the cost of UHPC production and its constituents warrants optimization of material use. Optimization of UHPC mixtures typically requires a large number of batch testing. Such an optimization approach is often time and cost intensive. Statistical techniques are efficient in terms of effort, time, and cost. A well-designed experiment can provide decisive conclusions on the optimization of mixture components with a minimum number of trials. Therefore, researchers have utilized statistical techniques to determine mixture designs that are cost-effective and eco-friendly. Ghafari et al. proposed an innovative analytical method based on a statistical mixture design (SMD) approach (Ghafari, Costa, and Júlio, 2015). The objective of employing this method was optimizing UHPC mixtures to obtain high compressive strength and suitable workability as well as minimizing cement consumption to ensure eco-efficiency. The researchers opted for a D-optimal design strategy with clearly defined upper and lower bounds of the mixture components. A D-optimal design is a computer-generated design in which the variance of the model coefficients is minimized. This is done by maximizing the determinant of the information matrix $X'X$. Here, X is the design matrix of the model terms and $X'$is the transpose of X. The "D" in the terminology stands for the determinant of the information matrix (Montgomery, 2017). Then based on a D-optimal mixture experiment, a 53-run D-optimal design was generated. Following experimental runs, an analytical model was constructed. This model encapsulated the relationship between the mixture components and concrete properties. Finally, through optimization of the analytical model, an eco-efficient mixture design with desired performance characteristics was achieved. They hypothesized that by using this technique, a UHPC mixture with compressive strength exceeding 150 MPa (21.75 ksi) without heat curing can be formulated.

Response surface methodology (RSM) is another statistical approach to develop UHPC mixtures with specific performance goals (Ferdosian and Camões, 2017; Li, Lu, and Gao, 2021; Zhou et al., 2021). In many cases, where a theoretical model relating factors (independent variables) and responses (output) is complex or not available, such relationships are sought by empirical RSM. The RSM generates knowledge in the experimental domain of interest and can reliably estimate experimental variability. RSM starts with clearly defining the problem and by selecting appropriate factors and levels. The design should efficiently describe the experimental space by using factorial, fractional factorial, central composite design, Box-Behnken design etc. This technique is most commonly used in conjunction with central composite design (CCD).

As shown in Figure 2.1, the CCD design incorporates factorial, axial, and center points encompassing the design space. The factorial points, representing the corners of the design space, are placed at all combinations of each factor's high and low levels. These levels are coded as +1 and -1, respectively. For a two-factorial design, the factorial points correspond to the four corners of a square in a 2-D space. The center points are the replicated runs at the midpoint of the design space. At center points all factors are set to their mid-levels and coded as 0. The axial points are located at a certain distance, α, from the center point (Sarabia, Ortiz, and Sánchez, 2020).

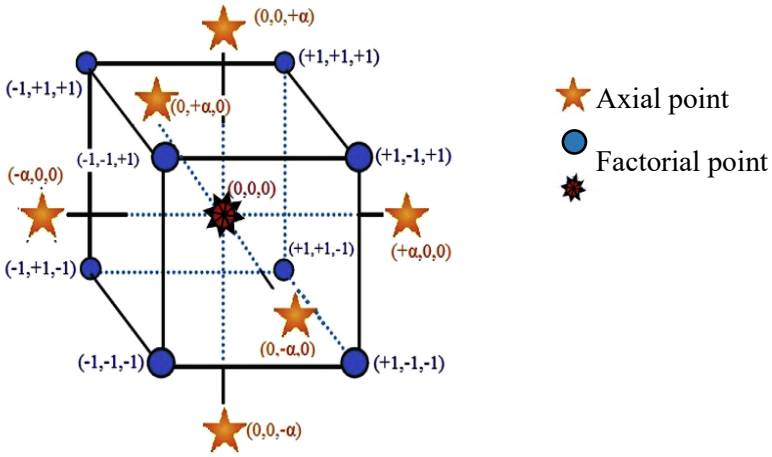

Figure 2.1 Schematic representation of factorial, axial, and center points in CCD. Adopted from Ferdosian and Camões (2017)

There are three types of CCD designs: 1) circumscribed (CCC), 2) inscribed (CCI), and 3) face centered (CCF) (Central Composite Designs [CCD], 2024). These types are schematically presented for two factors in Figure 2.2. The CCC design is the basic form of central composite design and was discussed in the previous paragraph. The CCC design is useful when the factor levels (low and high levels) are not the true limits. In such cases, the axial points set new low and high settings or levels for each factor. The CCI design is a scaled down CCC design. In this design, the factor levels are true limits. In CCI design, the factor levels are used as axial points. The factorial or fractional points are created within those limits. In CCF design, the axial points are at the center of each face of the factorial space.

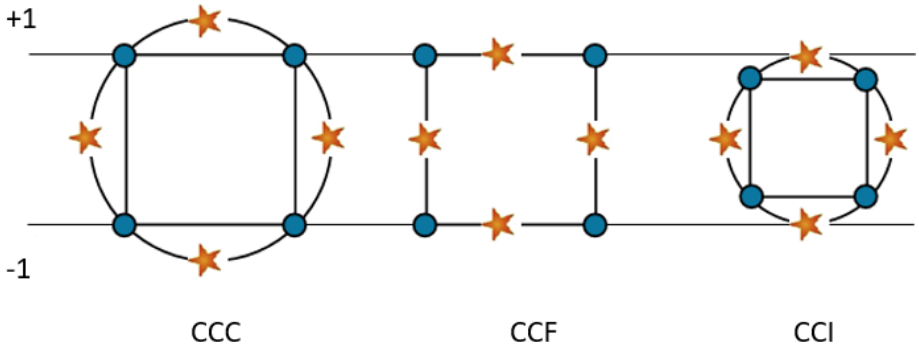

Figure 2.2 Three types of central composite design

Experiments are then conducted over the defined design space and the data are analyzed by fitting into mathematical models. For example, the experimental data can be fitted in a polynomial model, as shown in (Eq. 4).

$$Y = \beta_o + \sum \beta_i X_i + \sum \beta_{ii} X_i^2 + \sum \beta_{ij} X_i X_j + \epsilon$$

Where,
Y = Predicted response such as compressive strength
X_i, X_j = Factors such as water-to-binder ratio, etc.
β_o, β_i, β_{ii}, β_{ij} = Intercept, linear coefficients, quadratic coefficients, coefficients for interaction terms, respectively.
ϵ = Random error term that accounts for the experimental error assumed to have a normal distribution with mean zero and variance σ^2. (Eq. 4)

The estimation of variance (σ^2) can be estimated by (Eq. 5).

$$s^2 = \frac{\sum_i (y_i - \hat{y}_i)^2}{N - p}$$

Where,
s^2= Estimation of variance σ^2
y_i= Experimental values of the response
$\hat{y}_i$= Predicted value of the response
$N =$ Number of experiments
$p =$ Number of unknown parameters (Eq. 5)

This estimation of variance is dependent on the model. If the fitted model is inadequate, the estimated s^2 loses its significance. If more than one run at a certain design point is available, then a model independent estimation of variance can be obtained. As such, the center points are replicated to estimate the pure error for the lack of fit test and reduce the standard errors of the prediction. The model fitting includes regression analysis, evaluation of the significance of each model's terms using ANOVA, model adjustment and transformation, and diagnostic checking (Sarabia, Ortiz, and Sánchez, 2020). This model can be utilized from prediction of material properties and development of UHPC mixture with specific performance goals (Ferdosian and Camões, 2017; Li, Lu and Gao, 2021). A flowchart of utilizing RSM is provided in Figure 2.3.

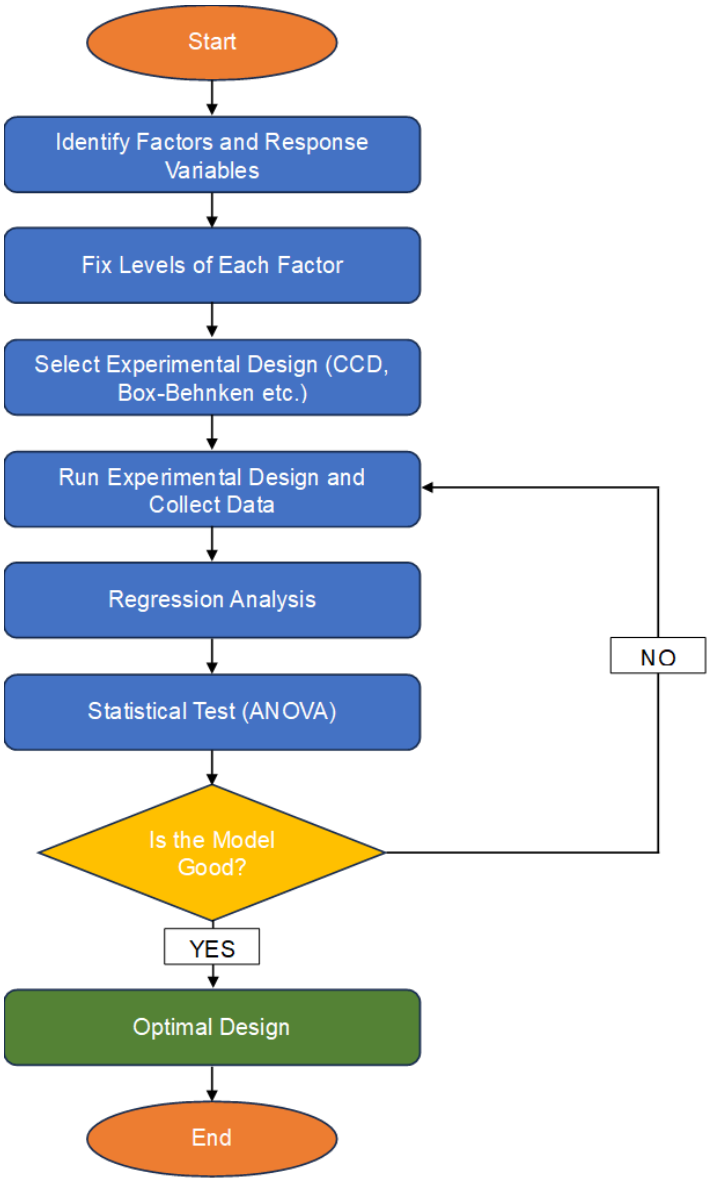

Figure 2.3 Optimization of mixture design with response surface methodology

2.5 Curing

Curing plays a critical role in UHPC production as it intensifies the pozzolanic reaction and improves the microstructure of the matrix during the material's early age. Curing method and duration are known to affect the mechanical and durability properties of UHPC (Prem, Ramachandra Murthy, and Bharatkumar, 2015; Zhang et al., 2018b; Shen et al., 2019; J. Li et al., 2020).

Since the innovation of reactive powder concrete (RPC), a precursor of UHPC, the significance of specialized treatment of the UHPC samples has been recognized. Elevated temperature intensifies the pozzolanic reaction and reduces porosity (Cheyrezy, Maret, and Frouin, 1995). At high curing temperatures ranging from 250°C (482°F) to 400°C (752°F), the transformation of amorphous cement hydration products into crystalline products has been reported, and the presence of xonotlite has been confirmed using XRD analysis (Richard and Cheyrezy, 1995; Sadrekarimi, 2004). Although a few hours

of steam curing normal concrete reduces the ultimate strength, the prolonged steam curing in UHPC can have a positive effect on compressive strength due to the extended pozzolanic reaction (Aydin et al., 2010). Improvement of the compressive strength by applying pressure on fresh samples has also been stated. Without pressure, RPC compressive strength has been reported to reach 488 MPa (70,780 psi) and 524 MPa (76,000 psi) at 250°C (482°F) and 400°C (752°F), respectively. By applying pressure before and during setting, compressive strengths of 631 MPa (91,520 psi) and 673 MPa (97,610 psi) at 250°C and 400°C, respectively, have been achieved for RPC (Richard and Cheyrezy, 1994, 1995). Although RPC compressive strength can be improved by pressing fresh samples, it results in an increase of specific weight and cost of production. More modern trends of UHPC production rely only on heat treatment or standard curing (Wille, Naaman, and Parra-Montesinos, 2011) Some of the common curing techniques are heat curing, steam curing, water curing, and autoclave curing. (Hamada et al., 2022).

Hiremath and Yaragal investigated four different curing regimes: ambient air curing, hot air curing, hot water bath curing, and accelerated curing by keeping water curing as control (Hiremath and Yaragal, 2017). For the ambient and hot water bath curing, the specimens were kept at 24±5°C (75 ± 9°F) and 90°C (194°F), respectively. For hot air curing, 100°C (212°F), 150°C (302°F), and 200°C (392°F) temperatures were chosen. The accelerated curing process involved keeping them in a moist environment with at least 90% humidity at 27 ± 2°C (80.6 ± 3.6°F) after their creation, followed by immersion in boiling water at sea level conditions (100°C), and subsequently cooling in a tank at 27 ± 2°C (80.6 ± 3.6°F). They reported that accelerated curing up to three hours produced the highest compressive strength. With increasing temperature, the strength was observed to increase for hot air curing. For a combined curing condition (12-hour hot water curing followed by seven days of hot air curing), the highest compressive strength of 180 MPa (26.1 ksi) was achieved. Xu et al. reported a slightly higher hydration degree of UHPC after three days of steam curing compared with 28 days of standard curing (Xu et al., 2022). They also demonstrated that the steam curing technique can reduce porosity by 34.4%. Another study by Prem et al. found steam curing to be beneficial for early-age strength development (Prem, Ramachandra Murthy, and Bharatkumar, 2015). However, at later stages, no enhancement was observed by XRD analysis, compared to water curing. They reported heat curing as the optimal approach for achieving maximum strength. A similar observation was made by Mo et al. (Mo, Gao, and Su, 2021). They reported significant enhancement of early-age UHPC compressive strength steam cured at 55°C (131°F) for 24 to 48 hours. However, they reported significant degradation of strength development at the end of the steam curing period. Another curing method frequently described in the literature is autoclave curing. In this method, specimens are exposed to high temperatures and pressure inside an autoclave chamber. Chen et al. reported that autoclave curing can improve UHPC compressive and flexural strength 37.5% and 30.3% compared with normal curing (Chen, Gao, and Ren, 2018).

Wille et al. explored the development of UHPC to attain high strength and ductility without special curing such as heat or pressure treatment (Wille et al., 2012). They emphasized optimizing the packing density of the cementitious matrix and using high-strength steel fibers, tailoring fiber geometry, and optimizing matrix-fiber interface properties. Their research reveals that with proper design and mix composition, it is possible to achieve UHPC with compressive strengths exceeding 150 MPa (22 ksi) and significantly improve durability without needing any special treatment. This promises more cost-effective onsite application of the product compared with currently available alternatives.

2.6 Properties of UHPC

Ultra-high-performance concrete has been engineered to achieve superior mechanical and durability properties compared with conventional concrete. Previous sections describe UHPC material composition, mixture design, and production techniques. This section provides an overview of the defining properties.

2.6.1 Fresh Properties

The most reported fresh property of UHPC is workability. Due to the low water-to-binder ratio, achieving a flowable paste requires careful proportioning and admixtures. Yu et al. reported that, compared with a single type of fiber, hybrid fibers show relatively good flowability (Yu, P Spiesz and Brouwers, 2015). They hypothesized that the long fibers could form imaginary borders to the short fibers. As such, the rotation of short fibers is resisted. This resulted in the reduction of resistance force to flow. Moreover, the short fibers can restrict the rotation of the long fibers as well. Hung et al. reported that the inclusion of silica sand and varying fiber content significantly affects the workability of UHPC mixtures (Hung, Chen, and Yen, 2020). They showed that higher silica sand content improved the workability of the mixture. They attributed it to the reduced inter-particle friction and increased free moisture. The addition of hooked-end steel macro fiber at a volume fraction of 1% increased the workability. However, this observation contrasted with the one related to straight steel macro fibers. They reported that while higher silica sand content and 1% hooked-end steel macro fibers by volume enhanced the flowability and deformability of the mixture, increasing fiber content adversely affected these properties. Feng et al. reported a slight improvement of workability with increasing recycled sand content (Feng et al., 2023). They attributed this to the pre-wetting of the aggregates to saturated surface dry conditions. On the other hand, nano-SiO_2 and nano-Al_2O_3 negatively affected the fluidity due to increased water adsorption. However, two other nano-materials, nano-$CaCO_3$ and nano-Fe_3O_4, slightly enhanced the fluidity. Su et al. investigated how different types of accelerators impact the fresh properties of UHPC (Su et al., 2021). They reported that with increasing the dosage of accelerators, the setting time and fluidity of the mixtures decrease. This trend held true for all four types of accelerators investigated in their research. This is because of the rapid formation of hydration products in the presence of accelerators, which absorb free water from the mixture.

2.6.2 Mechanical Properties

Compressive strength is the main UHPC mechanical property. In fact, all UHPC definitions refer to a certain level of compressive strength (ASTM C1856/C1856M, 2017; ACI 239R, 2018; FHWA, 2023). As discussed in previous sections, the strength of UHPC is a function of water-to-binder ratio, packing of material, pozzolanic reactions from SCMs, and method of curing. Some researchers have reported improvement of compressive strength by addition of fibers. Wu et al. reported that by using steel fiber reinforcement, the static compressive strength of UHPC mixtures can be increased by 20% to 46% (Wu et al., 2017). They also reported positive effects of fiber hybridization on compressive and flexural UHPC properties. The enhancement of compressive strength by adding 2% long fibers compared with 2% short fibers was reported to be significantly higher. Ahmad et al. also stated the positive effect of fibers on compressive strength and modulus of elasticity (Ahmad et al., 2019). However, no significant strength enhancement was observed beyond 3.1% fiber content. Le Hoang and Fehlin reported no noticeable change in compressive strength and elastic modulus by adding fibers (Le Hoang and Fehling, 2017). However, the post-peak branch of the stress strain curve is significantly influenced by fibers.

Shafieifar et al. reported the average tensile strength of 20.7 MPa (3ksi) from splitting tensile test (Shafieifar, Farzad, and Azizinamini, 2017). This is markedly higher compared with the tensile strength of normal concrete (3.5 MPa or 0.48 ksi). UHPC specimens show considerable capacity to sustain load even after initial cracking. This higher tensile strength and post-cracking behavior is attributed to the fiber bridging across cracks. Kalthoff et al. reported significant improvement of tensile strength under heat treatment and autoclave curing (Kalthoff, Raupach, and Matschei, 2021). Also, they investigated the effect of storage and surface humidity on tensile strength. They reported that alternating between water storage and 65% relative humidity dramatically decreased tensile strength. This is more significant for specimens stored at 65% relative humidity. However, the low tensile strength of dry-stored specimens can be restored by subsequent water storage. The geometry, surface area, volume fraction, and shape of fibers

also influence the workability and tensile strength of UHPC. Yang et al. reviewed the effects of fibers on the mechanical properties of UHPC (Yang et al., 2022). They also highlighted the critical role of fiber volume fraction, size, shape, orientation, distribution, bonding strength are critical for UHPC tensile strength. Increasing fiber content improves tensile strength up to a critical volume fraction, beyond which negative effects occur. This critical volume fraction is not fixed and reported to be 2 to 6% by different researchers. Smaller diameters and larger aspect ratios improve tensile strength and strain hardening but must remain within optimal ranges, typically less than 100. They noted that most of the research focuses on fiber volume fraction. Therefore, further research are required on the effect of size, distribution, orientation of fibers. Gurusideswar et al. investigated five different UHPC mixes under various strain rates (Gurusideswar et al., 2020). These mixes included micro steel fibers and industrial waste products. They reported up to a 300% increase in tensile strength under quasi-static loading conditions when micro steel fibers are added. Their study reveals that binary UHPC mixes are more sensitive to strain rates compared with ternary and quaternary mixes.

2.6.3 Shrinkage

Concrete shrinks as it dries out due to the loss of moisture. Soliman and Nehdi explored the shrinkage behavior of UHPC at early ages under different temperatures and humidity ranges of (Soliman and Nehdi, 2011). They reported that autogenous shrinkage is a temperature dependent phenomenon. Specimens exposed to higher temperatures experience a greater degree of shrinkage. They demonstrated that both autogenous and drying shrinkage are interconnected phenomena. They also explored the effect of shrinkage reducing admixtures (SRA) and a superabsorbent polymer (SAP) in mitigating shrinkage. They found that both SRA and SAP significantly reduce shrinkage under sealed conditions. Under drying conditions, SRA is effective in reducing drying shrinkage. However, SAP tended to increase it. Their research also indicated that the conventional assumption of the additive nature of drying and autogenous shrinkage may overestimate actual autogenous shrinkage under drying conditions. Yalçınkaya and Yazıcı reported that ground granulated blast furnace slag markedly increases both early age autogenous and drying shrinkage (Yalçınkaya and Yazıcı, 2017). They also reported that the type and amounts of mineral admixtures, curing condition, and relative humidity are the influential factors of UHPC shrinkage. Fu et al. found that a lower water-to-binder ratio or a higher fly ash content can reduce drying shrinkage in UHPC (Fu et al., 2022). However, superplasticizer and silica fume adversely affect drying shrinkage. They revealed that the effect of steel fibers on shrinkage is not monotonic. Amounts lower or higher than the optimum dosage of steel fiber (50 kg/m^3) lead to increased drying shrinkage. Among the factors investigated, the water-to-binder ratio is reported to have the most substantial effect on drying shrinkage. As the water-to-binder ratio affects the pore structure and distribution, this in turn influences shrinkage behavior.

2.6.4 Durability

Chloride ion penetration, one of the durability issue sources of concrete structures, is a process where chloride ions infiltrate the porous structure of concrete. This is a major concern in Utah as chloride ions from deicing salts compromise the durability of concrete structures and increase maintenance costs, reduce service life, and, most importantly, pose a safety risk.

Saladi et al. reported a significantly higher electrical resistivity of UHPC-class materials compared with conventional concrete (Saladi et al., 2023). Their research suggests that a denser microstructure is effective in lowering chloride ion penetrability. They demonstrated a strong inverse correlation between electrical resistivity and the chloride migration coefficient. According to Hasan et al., the chloride ion penetrability of UHPC specimens is influenced by a water-to-binder ratio and curing regime (Hasan, Allena, and Gilbert, 2024). They reported that the electrical resistivity varied from 49 to 1419 Ω-meter and conductivity from 0.0007 to 0.0013 millisiemens per meter. This indicates a very low to moderate

expected corrosion rate for the mixtures. Their results underscore that UHPC mixtures with water-to-binder ratio up to 0.3 show impressive corrosion resistance. Mousavinejad and Sammak reported that fibers can improve UHPC durability against chloride ion penetration (Mousavinejad and Sammak, 2021). In their paper, they conducted a rapid chloride penetration test, electrical resistivity, and a rapid chloride migration test. According to tests results, the mixtures with combined steel fibers and polypropylene fibers showed the least chloride ion penetration and highest resistance in rapid chloride migration tests.

Another durability issue source in Utah is the freezing and thawing action in winter weather. During freezing conditions, the transformation of water from a liquid to solid state can increase hydrostatic pressure inside concrete. Thus, exposure to freezing-thawing cycles can result in cracking, spalling, and surface scaling. Hasnat and Ghafoori demonstrated that UHPC has remarkable resistance to deterioration caused by freezing-thawing cycles (Hasnat and Ghafoori, 2021). UHPC containing Class F fly ash and silica fume exhibited the best performance. Straight steel fibers significantly enhanced the freeze-thaw resistance compared with hooked fibers. They also demonstrated that pozzolanic reactions can cause post freeze-thaw cycle strength-gain under favorable conditions. Lu et al. reported that reduced water-to-binder ratio improves UHPC's freeze-thaw resistance (Lu et al., 2021). They recommended the optimum contents of steel fiber, silica fume, and fly ash are 25–50 kg/m^3, 80–130 kg/m^3, and 60–100 kg/m^3, respectively. Beyond these limits, the freeze-thaw resistance can be negatively affected.

2.7 Field Application

UHPC mixtures have been investigated for decades for structural rehabilitation, improving bridge deck joints, overlays in deteriorated bridge decks, and other conditions. In some instances, the material has been used for constructing full scale structural elements such as bridge decks, girders, and piles. It has been successfully utilized to enhance the durability and performance of existing concrete bridges through cast-in-situ rehabilitation schemes using standard equipment (Brühwiler, Denarié, and Habel, 2005). For example, UHPC has been used for replacing wood bridge decks in the Netherlands, for durability-oriented applications in France, and for architecturally oriented applications in the USA. (Acker and Behloul, 2004; Kaptijn and Blom, 2004).

Two "world's first" UHPC road bridges were completed in France in 2001. The UHPC mix had a compressive strength of 170 MPa (24,650 psi) and a direct tensile strength of 8 MPa (1,160 psi). A 3% straight steel fiber content by volume was used to achieve ductile behavior. The longitudinal and transverse bending, tangent loading, and prestressing transfer length were verified for both serviceability and ultimate limit states. Before starting the construction phase, the prestress distribution and new concrete characterization were checked and verified by constructing and testing a beam component. Flexural tests were done on sawn prisms taken from the actual structure. Flexural tests on a monolithic slab and on a slab with a construction joint were performed to validate the transverse loading behavior of the deck. The viscous and self-leveling nature of the mix meant that no additional vibration was required, which made the concreting work simple. The mixing duration and behavior control of fresh UHPC were reported to be the primary considerations for construction of the beams in a precast plant. The beams were cured under 20°C (68°F) saturated environment without any heat treatment. A ready-mix batching plant was utilized for in-situ concreting, which was identical to the precasting work. No water seepage or cracks were identified when the beams were inspected approximately two years after construction of the first bridge. By that time, the bridge had been open to traffic for one year (Hajar et al., 2004).

In 2003, Iowa Department of Transportation funded a project to demonstrate UHPC use in bridge replacement. This project utilized Ductal®, a patented UHPC mix, with an expected 28-day compressive strength of 207 MPa (30,000 psi). Local precasters raised concern about the high cost of the mix, longer time required to batch the mix and additional cleaning time, possibility of damaging mixing equipment due to a high mixing energy requirement, modifications of form to account for high shrinkage value of the

mix compared with standard mixes, longer curing and setting time, and lack of appropriate testing equipment (Moore and Bierwagen, 2006).

Since then, UHPC use in the United State has gradually increased. According to the FHWA, as of December 2021, there were 342 instances of UHPC deployment in highway bridge construction. About 78% of those are connections between prefabricated elements, about 9% are link slabs, and about 4.7% are bridge deck overlays. One noticeable fact is the lack of full-scale deployment of UHPC in bridge or structural members. Only 1.75 % of the deployments are for precast/prestressed girders, piles, and decks (FHWA, 2023).

The material's high cost, in general, limits UHPC application to where the material properties are best utilized (Brühwiler, Denarié, and Habel, 2005). Therefore, production of UHPC and UHPFRC mixes with low-cost, locally available materials has been gaining importance across DOTs.

Mixing and placement of UHPC in the field remains a challenge for locally produced UHPC. Lawler et al. developed a locally available, low-cost UHPC mix for Florida precast application. With 1.5% of straight steel fiber, their moist-cured mix achieves 126 MPa (18,300 psi) compressive strength and 31.4 MPa (3,100 psi) flexural strength. In the field trial, the one-day compressive strength for match-cure samples is reported to be 138 MPa (20,000 psi). Banking on the hot Florida climate for facilitating curing, in the field, the UHPC piles cast with the mix are covered only with tarps (Lawler et al., 2019).

During the field trial, when the UHPC is transported with a forklift mounted bucket without any agitation, thixotropic behavior and formation of "elephant skin" have been reported by Lawler et al. Better initial workability is reported when the fresh UHPC is transported by a mixing truck, which provides continuous and slow agitation. However, they also report a loss of flow toward the end of placement in such a scenario. Increased mixing truck speed for one minute before discharging helps to maintain workability during the entire placement process. High temperatures and light breezes may result in loss of workability and early age drying (Lawler et al., 2019).

A common feature of UHPC application in the field is the small volume of the material. This is due to the high cost associated with purchasing UHPC from the supplier and the need for specially trained contractors and workers. The optimized non-proprietary UHPC mix without fibers developed for the Michigan DOT costs \$392/m^3 (\$513/yd^3). Every 1% increase in steel fiber content by volume increases the cost by approximately \$394/m^3 (\$516/yd^3) (El-Tawil et al., 2016). A locally developed non-fiber UHPC for the Colorado DOT costs \$1,174/m^3 (\$1,535/yd^3). With 2.3% steel fibers, the cost is reported to be \$1,967/m^3 (\$2,573/yd^3) (Kim, 2018). A summary of commercially available UHPC by Alsalman et al. reports that the price of UHPC varies from \$1,496/m^3 to \$2,843/m^3 (1,956/yd^3 to \$3,718/yd^3) (Alsalman et al., 2020a).

3. EXPERIMENTAL PROCEDURE

3.1 Introduction

This section discusses the materials used for the development of non-proprietary UHPC, methodology for selecting and optimizing the mixture design, materials used, mixing, sample preparation, curing methods, and experimental procedures.

3.2 Materials

As discussed in the previous chapter, a wide variety of cements, SCMs, and admixtures are used in UHPC production. However, considering availability in the local market and ease of access, the materials selected for this study are: (1) ordinary Portland cement (Type I/II), (2) MasterLife SF 100 densified silica fume (SF), (3) Class F fly ash, (4) Granusil 7030 silica sand, and (5) MasterGlenium 3030 high range water reducing admixtures. The water content in MasterGlenium 3030 is 79.7%. The amount of water used during mixing is adjusted according to HRWR dosage. All these materials are procured from local suppliers and distributors. The cement and silica sand are purchased from Intermountain Concrete Specialties. Silica fume and superplasticizer are purchased from BASF. The Class F fly ash is sourced from Bridge Source. The particle size distribution of the granular and powder components of the mixtures are provided in Figure 3.1. The particle size distributions are obtained using a Mastersizer 2000 laser diffraction particle size analyzer. The particle size distribution of the sand is obtained from sieve analysis conforming ASTM C136 (ASTM C136, 2006). All the materials are collected from local suppliers and distributors.

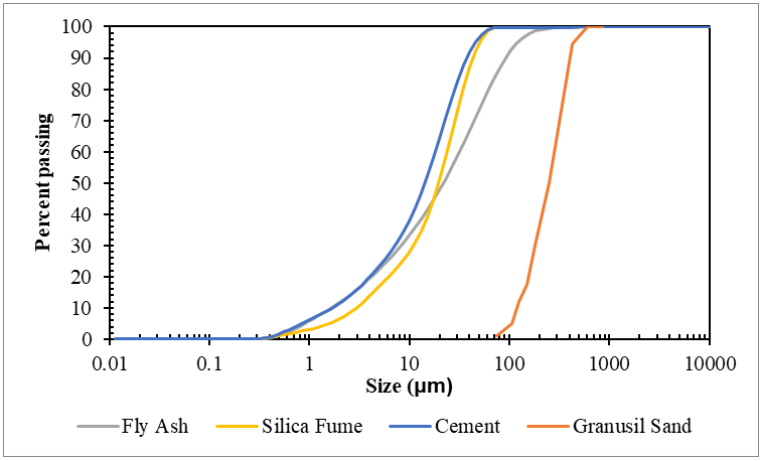

Figure 3.1 Particle size distribution of fly ash, silica fume, cement, and sand

3.3 Mixture Design

Depending on mixture design, UHPC ingredients, especially the supplementary cementitious materials and filler materials, can widely vary in types, composition, and gradation. Therefore, to identify the optimum dosage of mixture components, a response surface methodology (RSM) is opted for.

For this research, the range of the four selected variables are extensively studied (Allena and Newtson, 2011; Wille, Naaman, and Parra-Montesinos, 2011; Wille et al., 2012; Graybeal, 2013; Alsalman, Dang, and Hale, 2017; Soliman and Tagnit-Hamou, 2017; Meng and Khayat, 2018; Sadrmomtazi, Tajasosi, and

Tahmouresi, 2018; Wu, Khayat, and Shi, 2019; Nguyen, Thai, and Ngo, 2021). These four variables are water-to-cement ratio, silica fume-to-cement ratio, sand-to-cement ratio, and fly ash-to-cement ratio. The range of mixture components from the literature are presented in graphic format in Figure 3.2. Based on these ranges, the range of the mixture components (factors) are selected and presented in Table 3.1

The mixture designs are generated to populate the design points for an inscribed-type central composite design (CCD). These mixture designs are provided in Table 3.2. The inscribed type design is chosen because the limits of the factors are true limits for the mixture design. The mixture designs cover the ranges of ratios provided in Table 3.1.

Table 3.1 Range of factors (mixture components) for the experiment design with respect to cement

Cement	Water	Silica Fume	Fly ash	Sand
1	0.18–0.35	0.05–0.35	0–0.65	0.95–1.5

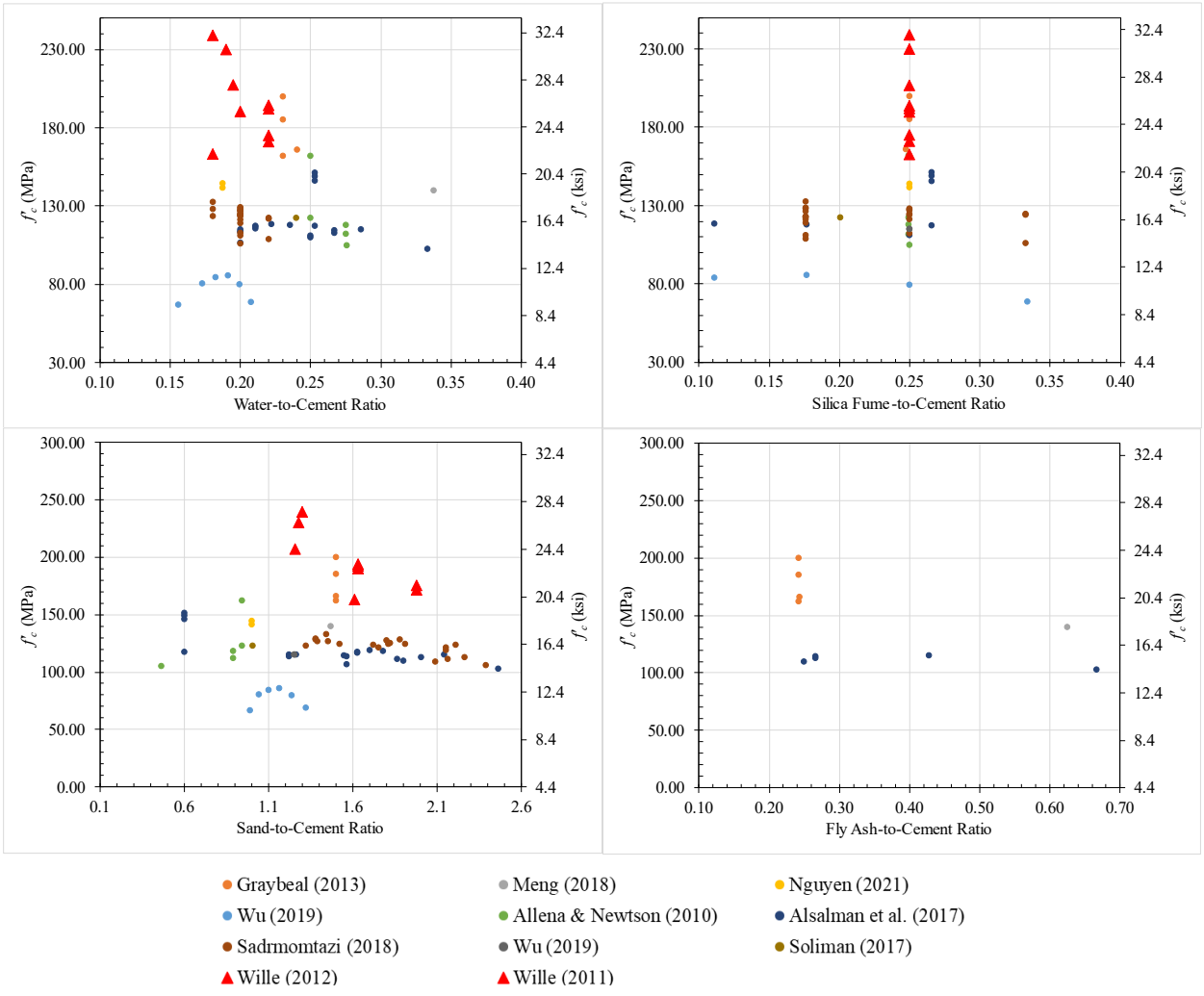

Figure 3.2 Range of mixture components to cement ratio from the literature

Table 3.2 Mixture design (1 kg/m^3 = 1.686 lbs./yd^3)

Batch ID	Cement (kg/m^3)	Water (kg/m^3)	Silica Fume (kg/m^3)	Fly Ash (kg/m^3)	Sand (kg/m^3)	HRWR (kg/m^3)
R1	932.70	207.53	116.59	151.56	1014.31	54.43
R2	864.19	265.74	108.02	140.43	939.80	50.43
R3	876.93	195.12	241.16	142.50	953.66	54.40
R4	816.10	250.95	224.43	132.62	887.51	50.637
R5	831.84	185.08	103.98	405.52	904.62	55.18
R6	776.91	238.90	97.11	378.74	844.89	51.54
R7	787.19	175.15	216.48	383.76	856.07	55.12
R8	737.82	226.88	202.90	359.69	802.38	51.67
R9	850.39	189.21	106.30	138.19	1158.66	55.37
R10	793.07	243.87	99.13	128.87	1080.55	51.64
R11	803.79	178.84	221.04	130.62	1095.16	55.30
R12	752.38	231.36	206.91	122.26	1025.12	51.76
R13	765.74	170.38	95.72	373.30	1043.32	55.97
R14	718.94	221.08	89.87	350.49	979.56	52.55
R15	727.74	161.92	200.13	354.77	991.55	55.88
R16	685.35	210.74	188.47	334.11	933.79	52.62
R17	790.12	209.38	158.02	256.79	967.89	53.39
R18	790.12	209.38	158.02	256.79	967.89	53.39
R19	847.00	152.46	169.40	275.28	1037.58	57.23
R20	740.39	259.14	148.08	240.63	906.98	50.03
R21	835.11	221.30	41.76	271.41	1023.01	53.35
R22	749.73	198.68	262.41	243.66	918.42	53.42
R23	880.57	233.35	176.11	0.00	1078.69	52.47
R24	716.52	189.88	143.30	465.74	877.74	54.14
R25	860.69	228.08	172.14	279.72	817.65	52.34
R26	730.24	193.51	146.05	237.33	1095.36	54.27
R27	790.12	209.38	158.02	256.79	967.89	53.39
R28	790.12	209.38	158.02	256.79	967.89	53.39

The mixture design includes 2^n = 16 factorial points, 2n = 8 axial (star) points, 1 center point. The center point is replicated three times. Here, n is the number of factors. In this case, n is equal to 4. In CCD design, central points are replicated to estimate the experimental error, verify the accuracy of the model, improve the precision of estimates, and detect lack of fit (Sarabia, Ortiz, and Sánchez, 2020). This led to a total of 28 mixtures shown in Table 3.2. From this ratio, the mixture designs are calculated using the process described by Neville (Neville, 1995). If the required quantities are water (W), cement (C), silica fume (SF), fly ash (FA), and sand (S), then for one cubic meter of concrete, we have:

$$\frac{W}{1000}+\frac{C}{1000\times SG_c}+\frac{SF}{1000\times SG_{SF}}+\frac{FA}{1000\times SG_{FA}}+\frac{S}{1000\times SG_S}=1$$

$$or,\quad \frac{W/C}{1000}+\frac{1}{1000\times SG_c}+\frac{SF/C}{1000\times SG_{SF}}+\frac{FA/C}{1000\times SG_{FA}}+\frac{S/C}{1000\times SG_S}=\frac{1}{C} \qquad \text{(Eq. 6)}$$

Here, SG is the specific gravity of the ingredients. The specific gravity of cement, silica fume, fly ash, and sand are 3.15, 2.2, 2.33, and 2.65, respectively. For the center point of the central composite design, the ratios W/C, SF/C, FA/C, and S/C are 0.265, 0.2, 0.325, 1.225, respectively. These ratios correspond to the medians of the ranges given in Table 3.1. Plugging in these values, the cement content can be calculated from (Eq. 6). The mass of the other ingredients can be calculated by multiplying the cement content and the ratio of each ingredient. The dosage of the HRWR used is 2,340 mL/100 kg (36 fl. oz/cwt) of total dry ingredients. Specific gravity of the HRWR is 1.05. Note that these batches do not contain any fibers as in this stage of the research; the main concentration is the UHPC matrix optimization.

3.4 Mixing, Curing, and Specimen Preparation

Mixing of the 28 batches shown in Table 3.2 is done by using an Avantco MX10 tabletop mixer with 10 qt. capacity. The mixing sequence is as follows:

- Mix all dry ingredients – 5 minutes (low speed, 156 rpm)
- Add 1/2 water + mix – 3 minutes (mid speed, 258 rpm)
- Add 1/2 water + mix – 4 minutes (mid speed, 258 rpm)
- Add HRWR + Mix – 4.5 + 4.5 = 10 minutes (mid speed, 258 rpm)

Mixing sequences following other researchers (Wille, Naaman, and Parra-Montesinos, 2011) are also employed and found to have no significant differences in results. A picture of the mixed dry ingredients and mixing machine is provided in Figure 3.3.

The workability of the mixtures is measured immediately after mixing is complete, as described in section 3.5. Then, 3 × 6 inch (75 × 150 mm) cylindrical specimens for the compressive strength test are cast according to ASTM C1856 and ASTM C39 (ASTM C39/C39M, 2018). If fibers are added to the mix, it is done during the last 4.5 minutes of mixing. The specimens are kept in the laboratory under room temperature conditions for 24 hours. At the end of 24 hours, the specimens are demolded and placed in an oven at 90°C for steam curing until testing. Before testing, the specimens are removed from the oven and the loading planes are cut with a saw. All the specimens were tested at 28 days.

Figure 3.3 (a) Dry ingredients in mixing bowl, (b) tabletop mixing machine

3.5 Flowability

The flowability of the mixes are measured according to the ASTM C 1457 Standard Test Method for Flow of Hydraulic Cement Mortar (ASTM C1457, 2013). In this method (Figure 3.4), a brass mold is placed on a flow table made of brass and the mold is filled with layers of mortar paste of approximately 1 inch (25 mm). The mortar is tamped 25 times. Then the rest of the mold is filled and tamped in a similar manner. Excess mortar is cut off and a plane surface flush with the top of the mold is achieved with the help of a trowel. The sides of the mold and the table are cleaned. The mold and the flow table are wiped clean and dry. Then the mold is lifted away, and the table is dropped 25 times in 15 seconds. The mortar spread is measured with a caliper.

Figure 3.4 Flowability test

3.6 Compressive Strength

UHPC compressive strength is tested according to the ASTM C1856 standard specification (ASTM C1856/C1856M, 2017). The specification requires that only 75-mm (3-inch) diameter by 150-mm (6-inch) long cylindrical specimens be tested for compressive strength. The cylinders are required to be end-grounded in such a way that the finished ends do not deviate from perpendicularity to the axis by more than 0.5°. The standard does not allow using capping compounds and unbonded neoprene pads. Therefore, the end surfaces of the UHPC test specimens were cut and grounded with a saw. However, based on the assumption that the specimens' end preparation with saw was not as good as expected, few specimens were tested using a neoprene pad. These specimens demonstrated higher compressive strength, implying the significance of proper surface preparation. In absence of an end-grinder for 3 × 6-inch (75 × 150 mm) cylinders, 4 × 8-inch (100 × 200 mm) cylinders are cast for the optimized mixture. The surfaces of these larger cylinders are ground at the UDOT facility in Salt Lake City. For each mix design, three such cylinders are tested using a compression testing machine. The length and diameter of each specimen are measured before testing. The loading rate for the specimens is 1.0 ±0.05 MPa (145 ± 7 psi/s) (ASTM C1856/C1856M, 2017). The specimens and test setup are provided in Figure 3.5. In the initial phase of the research program, fibers were excluded from the mixtures due to cost considerations. However, small trial batches with fibers were cast to study the workability and incorporation of fibers in UHPC mixtures. Figure 3-5(c) shows a specimen with steel fibers from such trial batches.

Figure 3.5 Compressive strength test: (a) Specimens, (b) Tested UHPC specimen with no fiber (c) Tested fiber-reinforced UHPC specimens, (c) Specimen with saw-cut end during test, and (d) Specimen with saw-cut end and neoprene pad during test

3.7 Freeze-Thaw Durability

A freeze-thaw durability test is performed according to ASTM C666 standard specification. ASTM C666 describes two procedures for determining the resistances of concrete specimens to rapidly repeated cycles of freezing and thawing: rapid freezing and thawing in water (Procedure A), and rapid freezing in air and thawing in water (Procedure B). The test standard notes that neither of these test procedures are intended to provide a quantitative measure of the concrete's service period. Rather, these procedures are intended to quantify the effects of variations in properties and conditioning of freezing and thawing cycles. The test method does not provide any specific guideline on choosing either Procedure A or Procedure B. Procedure A is more aggressive, while some consider Procedure B to be more representative (ASTM C666/C666M, 2015).

For this research, Procedure A is chosen as it is considered to be more effective in revealing defective material. Cylindrical specimens, 4 × 8 inch (100 × 200 mm), are prepared for the test. A freeze-thaw chamber from Caron and an Emodumeter® from James Instruments are used to apply the freezing-thawing cycle on specimens and to measure the dynamic elastic modulus of the specimens. Figure 3.6

shows the freeze-thaw durability test specimens, chamber, and test setup. According to Procedure A, the specimens are required to be surrounded by a layer of water between 1/32-inch (1 mm) to 1/8-inch (3 mm) thickness. The specimens are submerged in the water during the testing period. The procedure involves alternately lowering the temperature of the specimens from 40°F to 0°F (4°C to -18°C) and raising it from 0°F to 40°F (-18°C to 4°C). Each cycle is completed within two to five hours. The fundamental frequencies are measured at an interval of less than 36 cycles. The relative dynamic modulus of elasticity (P_c) and durability factor (DF) can be calculated using (Eq. 7).

Figure 3.6 (a) and (b) Freeze-thaw durability test specimens, (c) Fundamental frequency and dynamic elastic modulus test setup, and (d) Freeze-thaw chamber with specimens

$$P_c = \left(\frac{n_1^2}{n^2}\right) \times 100$$

$$DF = \frac{PN}{M}$$

(Eq. 7)

Where,
$n_1 =$ *fundamental transverse frequency at* 0 *cycles of freezing and thawing*
$n =$ *fundamental transverse frequency after c cycles of freezing and thawing*
$P =$ *relative dynamic modulus of elasticity at N cycles, %*
$N =$ *number of cycles at which P reaches the specified minimum value for discontinuing the test or the specified number of cycles at which the exposure is to be terminated, whichever is less*
$M =$ *specified number of cycles at which the exposure is to be terminated*

ASTM C215 provides the equations to calculate the dynamic modulus of elasticity from both fundamental transverse and longitudinal frequencies as provided in (Eq. 8) (ASTM C215, 2014).

$$Dynamic\ E = CMn^2$$

$$\text{And, } Dynamic\ E = DM(n')^2$$

$$\begin{aligned}
&Where,\\
&M = mass\ of\ specimen, kg\\
&n, n' = fundamental\ transverse\ and\ logitudinal\ frequencies, respecitively, Hz\\
&C = \frac{1.6067 L^3 T}{d^4}, m^{-1}\ for\ a\ cylinder\\
&D = 5.096\left(\frac{L}{D}\right)^2, m^{-1}\ for\ a\ cylinder\\
&d = diameter\ of\ a\ cylinder, m\\
&L = length\ of\ specimen, m\\
&T = correction\ factor
\end{aligned} \qquad \text{(Eq. 8)}$$

3.8 Surface Electrical Resistivity Test

The surface electrical resistivity test is a non-destructive test used to estimate the resistance of chloride-ion penetration in concrete. This test is performed in accordance with the AASHTO T358 specification using 4 × 8-inch (100 × 200 mm) concrete cylinders. In this method, the resistivity to chloride-ion penetration of concrete cylinders is measured by using a 4-pin Wenner probe array. The testing apparatus sends a low frequency alternative current potential difference across the outer pin of the Wenner array. This results in a current flow through the concrete specimen. The potential difference between the outer and the inner probes is recorded. Three more measurements are taken by rotating the specimen by 90°. The average resistivity is then reported. The resistance to the chloride ion potential is then estimated from a table provided in AASHTO 385 (AASHTO T 358, 2021). The testing apparatus and a specimen are shown in Figure 3.7. Table 3.3 shows the relation of chloride penetrability classification and surface electrical resistivity at 73.4°F (23°C).

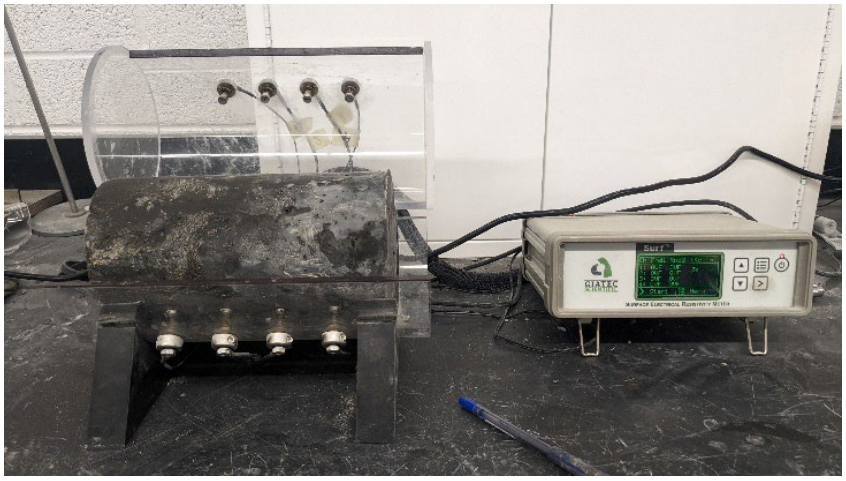

Figure 3.7 Surface electrical resistivity test setup

Table 3.3 Relation between chloride ion penetration and surface resistivity of concrete

Chloride Ion Penetration	Surface Resistivity Test	
	4×8-inch Cylinder (kΩ-cm) a = 1.5	6×12-inch Cylinder (kΩ-cm) a = 1.5
High	<12	<9.5
Moderate	12–21	9.5–16.5
Low	21–37	16.5–29
Very Low	37–254	29–199
Negligible	>254	>199
a = Wenner probe tip spacing		

3.9 Drying Shrinkage Test

Drying shrinkage test of UHPC specimens are performed following ASTM C157 specification. This test method describes the procedure to determine the length change of mortar and concrete specimens that are produced by causes other than externally applied forces and temperature changes under controlled environment. For this test, prismatic specimens of 3 × 3 × 11.25-inch (75 × 75 × 286 mm) are prepared as described in ASTM C1856. The specimens are demolded after 24 hours. Upon removal of specimens from the molds, they are placed in lime-saturated water to minimize the variation in temperature. The specimens are then wiped, and an initial comparator reading is taken. After that the specimens are cured until 28 days of age. At the end of the curing, a second comparator reading is taken. ASTM C157 describes two procedures for storage of specimens: water storage and air storage. In this research program, air storage is chosen. The specimens are stored at 50% relative humidity and 73±3°F (23±2°C) (ASTM C157/C157M, 2014; ASTM, 2017). The length change of any specimen at any age can be calculated using (Eq. 9). The test setup is presented in Figure 3.8.

Figure 3.8 Drying shrinkage test setup

$$\Delta L_x = \frac{CRD - initial\ CRD}{G} \times 100$$

$Where,$ (Eq. 9)
$\Delta L_x = length\ change\ of\ specimen\ at\ any\ age, \%$
$CRD = difference\ between\ the\ comparator\ reading\ of\ the\ specimen\ and\ the\ reference\ bar\ at\ any\ age$
$G = the\ gage\ length, 10\ inch\ (250\ mm)$

3.10 Autogenous Shrinkage Test

An autogenous shrinkage test is performed according to the ASTM C1698 test standard. In this test, the bulk strain of sealed cement pastes or a mortar specimen subjected to no external forces is measured. In this method, three specimens are prepared. The measurement starts at the time of the final setting. Corrugated molds are filled on a vibrating table. Then the specimens are sealed and horizontally stored in a temperature-controlled room at 73±3°F (23±2°C). The specimens are stored horizontally such that no restraint, damage, and dissipation of heat of hydration can occur. The measurement process involves the length measurement of specimens using a dilatometer bench. A reference bar is first inserted, and the gauge is reset to zero. Then the specimen is set on the dilatometer bench and the length is measured. Unless otherwise mentioned, the measurement is taken at the time of final setting and at one, three, seven, 14, and 28 days after mixing (ASTM C1698, 2019). The length change is calculated following (Eq. 10). An autogenous shrinkage specimen on the dilatometer bench is presented in Figure 3.9.

$$L(t) = L_{ref} + R(t) - 2 \times L_{plug}$$

$$\text{And, } \epsilon_{autogenous} = \frac{L(t) - L(t_{fs})}{L(t_{fs})} \times 10^6 = \frac{R(t) - R(t_{fs})}{L(t_{fs})} \times 10^6\ \frac{\mu m}{m}$$

$Where,$ (Eq. 10)
$L_{ref} = length\ of\ reference\ bar,\ mm$
$R(t) = reading\ of\ length\ gauge\ with\ specimen\ in\ the\ dilatometer,\ mm$
$L_{plug} = average\ length\ of\ end\ plugs, mm$
$L(t) = the\ length\ of\ the\ paste\ or\ mortar\ specimen\ at\ time\ t$
$\epsilon_{autogenous} = autogenou\ shrinkage\ strain$
$T_{fs} = time\ of\ final\ setting$

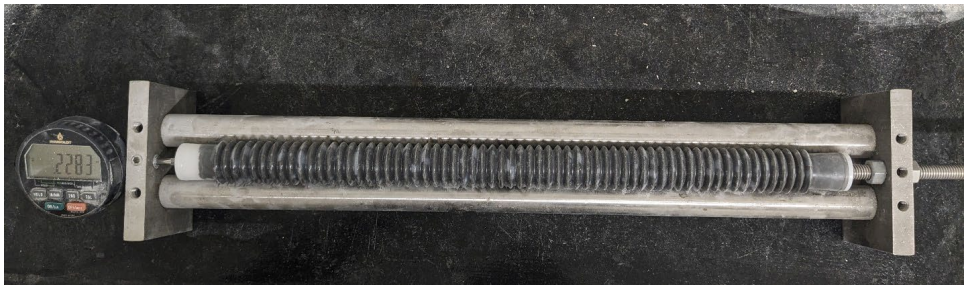

Figure 3.9 Autogenous shrinkage test specimen

4. RESULTS

4.1 Introduction

In this chapter, the findings from the experimental investigations conducted to evaluate the properties of UHPC mixtures are presented. The test program is divided into two phases: optimization of workable UHPC mixture to achieve the characteristic compressive strength using statistical technique, and evaluation of durability and volume stability properties of optimized mixture. The compressive strength data are used to perform a detailed statistical analysis using response surface methodology (RSM). The statistical model obtained from RSM is used to optimize the mixture proportion to achieve the target strength of non-proprietary UHPC developed for UDOT.

4.2 Flow Test

The flow test results of the 28 mixtures are presented in Figure 4.1. The flowability of the mixtures varies from 145.5 mm (5.73 inches) to 227.8 mm (8.97 inches) from mixture to mixture. It was found from the mixing and casting process that a mixture with flow value over 200 mm (7.9 inches) was desired for ease of mixing and casting. For mixtures with flow value below 190 mm (7.5 inches) was stiff and difficult to work with. However, Figure 4.1 does not provide a clear understanding of how the ratio of different ingredients affects the mixture's workability.

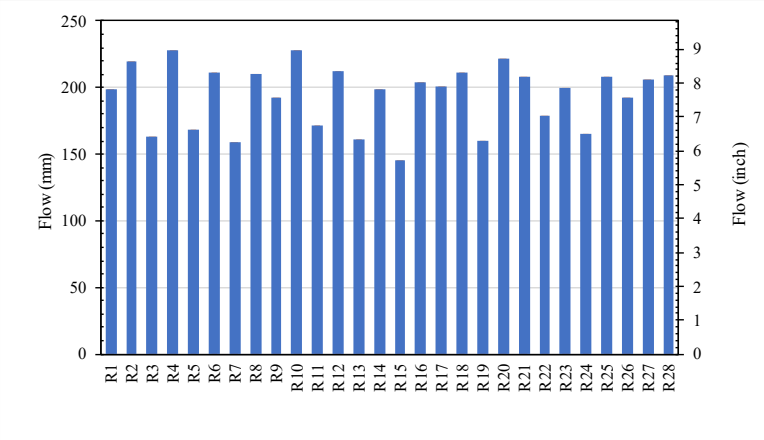

Figure 4.1 Variation of flow of UHPC mixtures

To investigate how the ratio of different ingredients influences the flowability of the mixture, flow is plotted against the ingredient-to-binder ratio and presented in Figure 4.2. From the plot, no clear pattern of flow behavior for cement-to-binder, silica fume-to-binder, fly ash-to-binder, and sand-to-binder ratio is observed. However, the flow versus water-to-binder ratio demonstrates a clear pattern. The flow steadily increases with the water-to-binder ratio. At a water-to-binder ratio of 0.17, the flow value is around 200 mm (7.9 inches). With increasing water-to-binder ratio, the flow value increases up to 227.8 mm (8.97 inches). As mentioned before, the most workable mixtures have a flow value of 200 mm (7.97 inches) and

above. Therefore, two conclusions can be made: (1) water-to-binder ratio is the main influencing factor for workability, and (2) 0.17 is the minimum water-to-binder required to maintain desired workability.

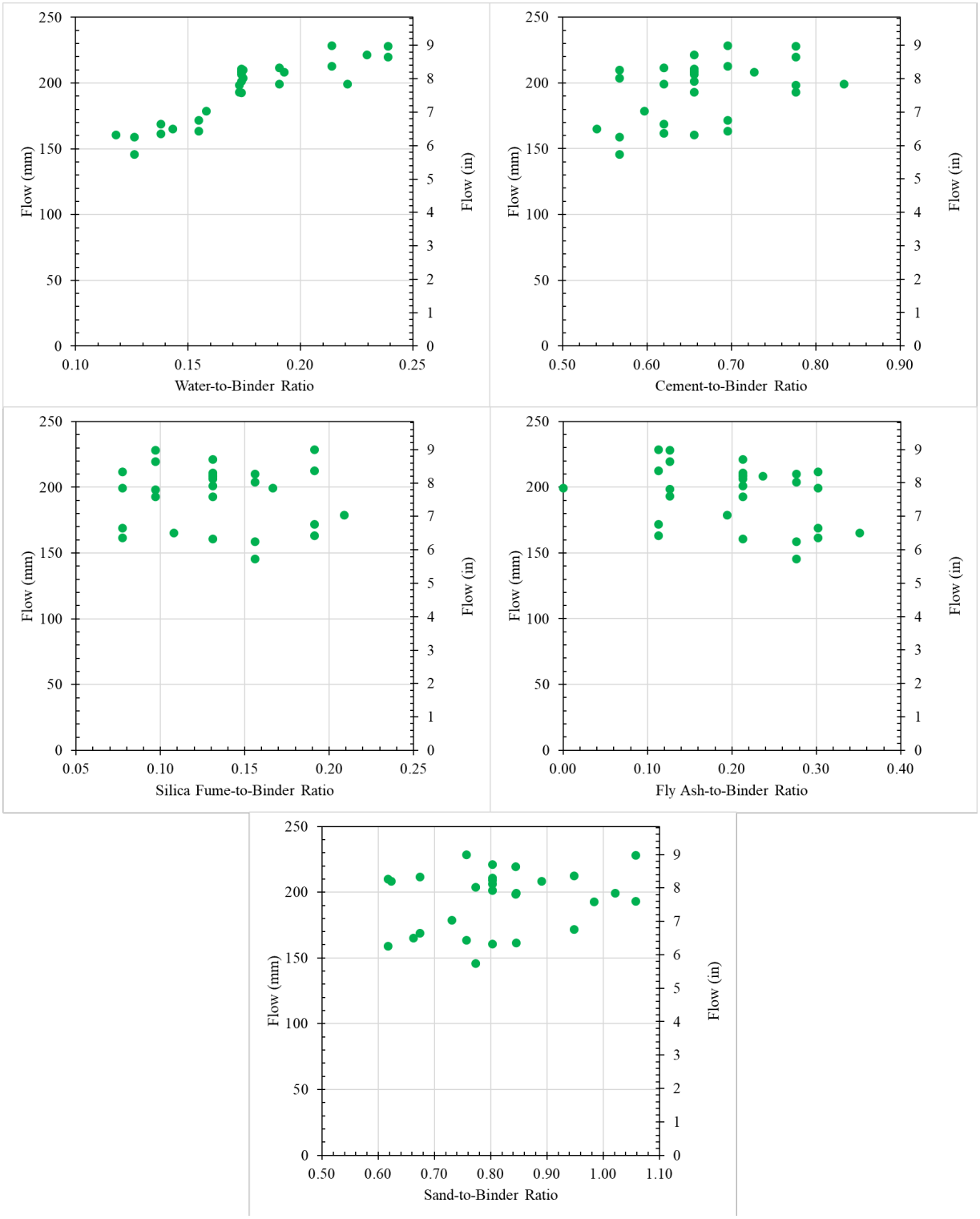

Figure 4.2 Variation of flow with mixture components to ratio

4.3 Compressive Strength

Compressive strength is the most important mechanical property of UHPC. As discussed in section 2.1, different agencies and standards set different limits of compressive strength to qualify a cementitious material as UHPC. Therefore, the focus of this research program's initial stage is to achieve the desired strength. Compressive strengths of the 28 mixtures are presented in Figure 4.3. All the specimens failed in cone or columnar pattern.

The compressive strength of different mixtures presented in Figure 4.3 shows that, at this point, none of the mixtures had sufficient strength to qualify as UHPC. The maximum strength of 114.6 MPa (16,628 psi) was achieved for mixture R25. However, similar to Figure 4.1, this plot does not reveal the contribution of different ingredients to compressive strength.

The variation of compressive strength with different ingredients-to-binder ratios is presented in Figure 4.4. It is observed that at very low water-to-binder ratios, the compressive strength is low. This can be attributed to a lack of sufficient water in the matrix for the hydration process. While a low water-to-binder ratio is one of the fundamental techniques of UHPC production, adequate water is required for hydration reaction. Alternatively, the strength of the mixtures reduces at higher water-to-binder ratios. From the plot, it is observed that the optimum water-to-binder ratio is 0.17.

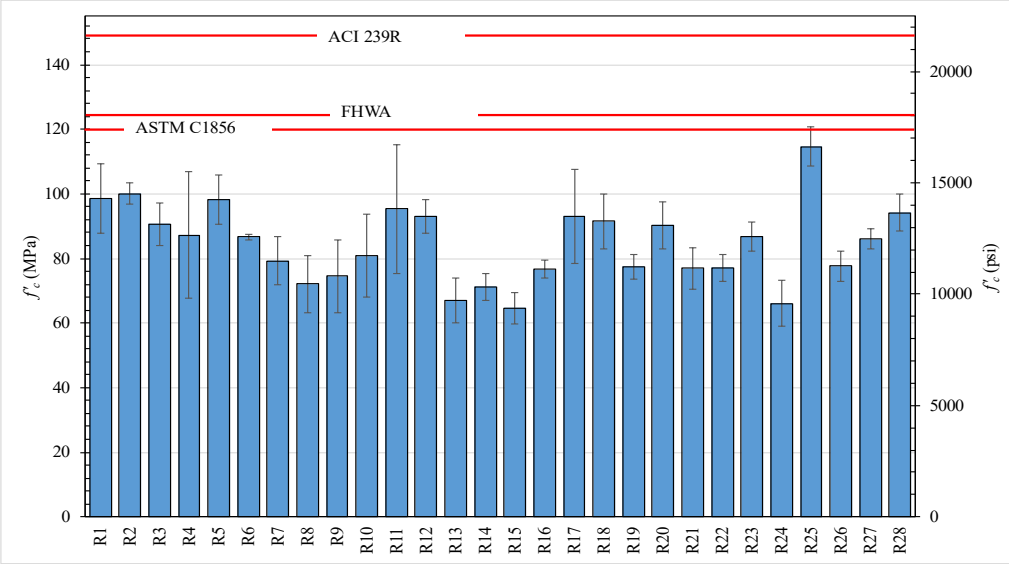

Figure 4.3 Compressive strength of the mixtures at 28 days. The red lines mark the minimum compressive strength limit set by different agencies

UHPC employs a higher cement content compared with conventional concrete. A high cement content is necessary to attain a high compressive strength by accelerating the hydration reaction (Alsalman et al., 2020b). As seen in Figure 4.4, the compressive strength gradually increases with increasing cement-to-binder ratio up to 0.66. However, beyond a ratio of 0.66, the compressive strength gradually decreases. Talebinejad et al. attributed this to the limited participation of aggregates in UHPC compaction at higher cement content (Talebinejad et al., 2004). From the experimental results, the maximum compressive

strength was achieved for 0.13 silica fume-to-binder ratio, 0.21 fly ash-to-binder ratio, and 0.62 sand to binder ratio. Note that the experimental program is designed in a way that statistical techniques are required to discern the contribution and optimum dosage of ingredients. Therefore, without performing statistical analysis, a conclusion on the optimization of the mixtures should not be reached.

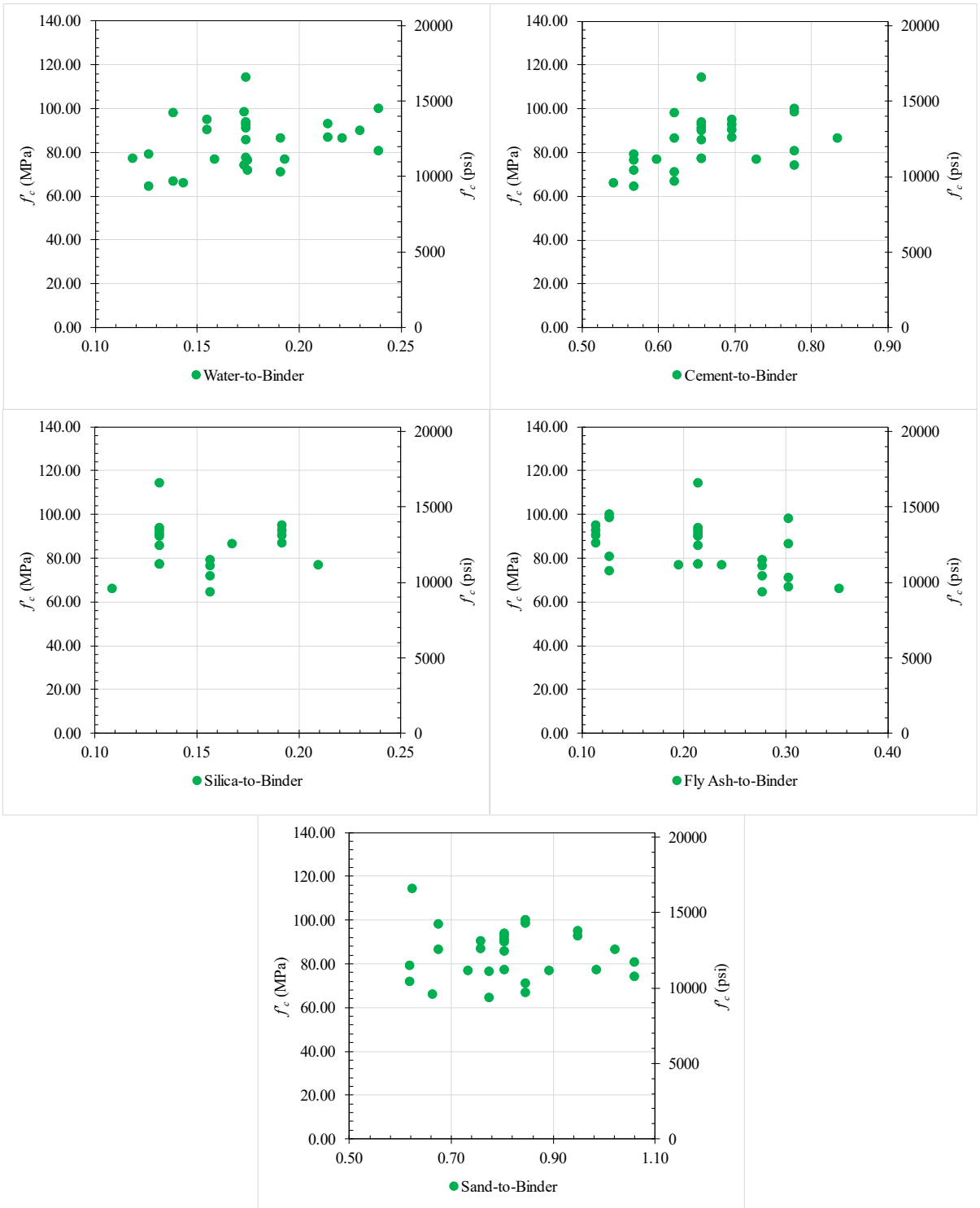

Figure 4.4 Variation of compressive strength with mixture components to binder ratio

The current standard and practice do not allow anything but end-grounded specimens for a compressive strength test of UHPC cylinders. However, it is difficult to achieve smooth loading surface by simply saw cutting the end of the specimens. Therefore, it was decided to test some specimens using neoprene pads with saw-cut loading surfaces. To this end, some cylindrical specimens from random batches were saved and tested with the above-mentioned setup. The compressive strength test results of these specimens and compressive strength of the specimens from the same batch but without the neoprene pads are presented in Figure 4.5. R30-LW was heat cured in limewater and denoted by "LW." With the neoprene pads, the maximum compressive strength of 152 MPa (22,076 psi) was achieved for batch R26. Note that without the neoprene pads, the strength of this batch was almost half. This indicates that the low strength achieved in earlier tests were likely due to loading surface preparation rather than deficiencies in the mixture design. However, using neoprene pads is not supported by recent standards and the literature. Despite this shortcoming, the results are promising in the sense that better preparation of the loading surfaces may help to achieve the desired strength of the mixtures. Therefore, at the end of this phase of experimental work, it was decided to utilize an end-grinder available at the UDOT facility. As discussed before, only 4 × 8-inch (100 × 200 mm) cylinders can be grinded with this end grinder. As such, 4 × 8-inch (100 × 200 mm) cylinders are cast for the optimized mixture. The development of this optimized mixture is discussed in section 4.4.

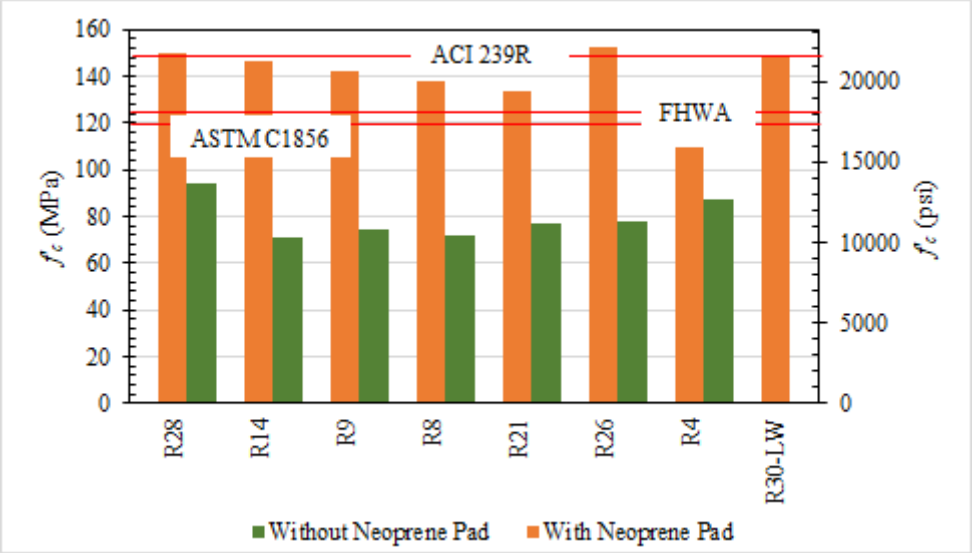

Figure 4.5 Compressive strength test results with neoprene pads at 28 days

4.4 Response Surface Model

The test results presented in Figure 4.3 were used to perform a detailed RSM analysis of UHPC, focusing on the effects of material ratios (water, silica fume, fly ash, and superplasticizer) on the mixtures' compressive strengths. Using Minitab, five different methods of fitting were considered: model including all terms (water-to-cement ratio, silica fume-to-cement ratio, etc.), forward elimination criteria, stepwise, forward selection, and backward elimination. The *forward information criteria* method adds the term with the lowest p-value to the model at each step. Additional terms can enter the model in one step if the settings for the analysis allow consideration of non-hierarchical terms but require each model to be hierarchical. The *stepwise* method starts with an empty model or includes the specified terms to include in the initial model or in every model. A term is then added or removed in each step. The process stops when all variables not in the model have p-values that are greater than the specified significance level, α. The *forward selection* method starts with an empty model or includes the specified terms to include in the

initial model or in every model. The most significant term is then added for each step. This stops when all variables not in the model have p-values that are greater than the specified α. The *backward elimination* method starts with all potential terms in the model and removes the least significant term for each step. The process stops when all variables in the model have p-values that are less than or equal to the specified α.

From these methods, the backward elimination was selected based on performance. The final model includes terms for water-to-cement (W/C), silica fume-to-cement (SF/C), fly ash-to-cement (FA/C), sand-to-cement (S/C), their squared terms, and certain interactions found to be significant. Notably, FA/C, S/C, $(SF/C)^2$, and $(FA/C)^2$ show high significance with p-values of 0.000, indicating a strong influence on the response variable. The coefficients indicate the direction and magnitude of each term's effect. For instance, a negative coefficient for FA/C and S/C suggests that increases in these ratios decrease the response (compressive strength), whereas positive coefficients for interactions indicate enhancement effects. The statistical analysis results are provided in Table 4.1.

Table 4.1 Statistical analysis results

Term	Coefficient	Standard Error	t-Value	p-Value	VIF
Constant	93.34	1.82	51.24	0.000	
W/C	1.86	1.78	1.04	0.311	1.00
SF/C	-0.89	1.86	-0.48	0.640	1.01
FA/C	-11.82	1.84	-6.43	0.000	1.00
S/C	-14.59	1.88	-7.75	0.000	1.01
$(W/C)^2$	-8.17	3.55	-2.30	0.034	1.06
$(SF/C)^2$	-15.18	3.57	-4.25	0.001	1.07
$(FA/C)^2$	-15.92	3.57	-4.46	0.000	1.06
W/C×S/C	9.49	4.36	2.18	0.044	1.00
SF/C×FA/C	-10.67	4.47	-2.39	0.029	1.00
SF/C×S/C	23.39	4.62	5.06	0.000	1.00

In Table 4.1, the coefficient values represent the change in the response variable (compressive strength) for a one-unit change in the predictor variable, assuming all other variables remain constant. For example, the W/C ratio coefficient is 1.86, indicating a slight positive impact on the response variable for every unit increase in W/C, but with a p-value of 0.311; this effect is not statistically significant. However, based on domain knowledge, this term was included in all steps of the analysis. Standard error indicates the accuracy of the coefficient estimates. Lower standard error values denote higher precision. For instance, the standard error for the constant term is 1.82, suggesting a relatively precise estimate of the constant term in the regression model. The t-value and p-values assess the significance of each coefficient. The p-values associated with each term tell whether the effects are statistically significant. For example, FA/C and S/C have p-values of 0.000, denoting their significant influence on the UHPC properties. Variance inflation factor (VIF) values near 1.00 for most terms suggest that multicollinearity is not significantly inflating the variance of the estimated coefficients. This indicates that the predictors in the model are relatively independent of each other, which is desirable for regression analysis. The fitted polynomial function is given in (Eq. 11).

$$f_c'(MPa) = 93.34 + 1.86\frac{W}{C} - 0.89\frac{SF}{C} - 11.82\frac{FA}{C} - 14.59\frac{S}{C} - 8.17\left(\frac{W}{C}\right)^2 - 15.18\left(\frac{SF}{C}\right)^2 - 15.92\left(\frac{FA}{C}\right)^2 + 9.49\left(\frac{W}{C}\right)\times\left(\frac{S}{C}\right) - 10.67\left(\frac{SF}{C}\right)\times\left(\frac{FA}{C}\right) + 23.39\left(\frac{SF}{C}\right)\times\left(\frac{S}{C}\right) \quad \text{(Eq. 11)}$$

Table 4.2 presents the model summary. R^2 and Adjusted R^2 values are high, indicating that the model explains a large proportion of variance in the response variable. The Predicted R^2 suggests good predictive power. The Standard Deviation value of 4.54 reflects the average distance of the data points from the fitted values.

Table 4.2 Model summary

Standard Deviation	R^2	Adjusted R^2	Predicted R^2
4.54	90.81%	85.41%	74.46%

Table 4.3 presents the analysis of variance (ANOVA), which is a critical component of RSM analysis. It provides insights into the significance of the model and its terms in predicting UHPC properties. The F-value and p-value for the overall model are indicators of the model's efficacy. The model has a very low p-value (0.000 for the model), suggesting that the model significantly predicts the response variable.

Table 4.3 Analysis of variance (ANOVA)

Source	Degree of Freedom	Adjusted Sum of Squares	Adjusted Mean Square	F-value	p-value
Model	10	3466.46	346.65	16.81	0.000
Linear	4	2119.97	529.99	25.70	0.000
W/C	1	22.46	22.46	1.09	0.311
SF/C	1	4.67	4.67	0.23	0.640
FA/C	1	853.06	853.06	41.36	0.000
S/C	1	1239.81	1239.81	60.11	0.000
Square	3	676.93	225.64	10.94	0.000
$(W/C)^2$	1	109.22	109.22	5.30	0.034
$(SF/C)^2$	1	372.32	372.32	18.05	0.001
$(FA/C)^2$	1	410.47	410.47	19.90	0.000
2-Way Interaction	3	742.58	247.53	12.00	0.000
W/C×S/C	1	97.79	97.79	4.74	0.044
SF/C×FA/C	1	117.67	117.67	5.71	0.029
SF/C×S/C	1	528.44	528.44	25.62	0.000
Error	17	350.64	20.63		
Lack-of-Fit	14	311.72	22.27	1.72	0.364
Pure Error	3	38.92	12.97		
Total	27	3817.10			

Linear terms (W/C, SF/C, FA/C, S/C) have their own sum of squares, degrees of freedom, and F-values, indicating their individual contributions to the model. The significant F-values and low p-values for FA/C and S/C confirm their strong influence on UHPC properties. Square terms and interaction terms are tested similarly, with their significance indicated by F-values and p-values. Notably, significant interactions like SF/C×S/C suggest complex relationships that enhance the model's predictive capabilities. The lack-of-fit test p-value is 0.364. This is higher than the threshold 0.05. Thus, the model does not suffer from a

significant difference in observed and predicted response. From the RSM model, three mixture designs are generated and shown in Table 4.4.

Table 4.4 Mixture proportion of the mixtures from RSM analysis

Cement-to-Binder	Water-to-Binder	Silica Fume-to-Binder	Fly Ash-to-Binder	Sand-to-Binder
0.73	0.16	0.065	0.21	0.70

In the next rounds of testing, further compressive strength tests were conducted using the optimized mixture design obtained from RSM analysis. The mixture proportion of the optimized mixture is presented in Table 4.5. In this phase, steel fibers were incorporated in the UHPC mixture to improve tensile behavior. The number in the batch ID refers to the fiber content by volume. The fibers selected for these mixtures are SikaFiber®-6513 UHPC. The length, diameter, and aspect ratio of these fibers are 13 mm (0.5 inches), 0.2 mm (0.008 inches), and 65, respectively.

Table 4.5 Mixture design of optimized UHPC

ID	Cement (kg/m^3)	Water (kg/m^3)	Silica Fume (kg/m^3)	Fly Ash (kg/m^3)	Sand (kg/m^3)	Fiber (kg/m^3)	HRWR (kg/m^3)
UHPC2	883.02	198.37	76.26	255.1	838.87	157.04	50.45*

*HRWR dosage was increased by a factor of 2 while using the IMER 360 Plus mixer.

Once the desired strength of the mixtures was achieved, further tests to quantify UHPC properties were conducted. These tests are the drying shrinkage tests, surface resistivity test, freeze-thaw resistance test, and autogenous shrinkage test.

4.5 Properties of Optimized Mixture

The optimized mixture UHPC2 from Table 4.5 was mixed and tested for long-term shrinkage and durability properties. In this section, the compressive strength, durability, and shrinkage properties of UHPC2 is presented.

4.5.1 Mixing Method

In this phase of testing, a larger volume of UHPC was cast. For this purpose, IMER 360 Plus, a high-shear vertical shaft mixer, was utilized. The mixer is shown in Figure 4.6. This mixer, with the help of three paddles, allows rotation through the mix rather than lifting and dropping it as conventional mortar mixers. Thus, this mixture is preferred for those with a low water-to-binder ratio—like UHPC. However, IMER 360 has a lower rotational speed (35 rpm) compared with the tabletop mixer described in section 3.4. This resulted in lower workability compared with the small batches mixed with the high-speed tabletop mixer. To overcome this issue, the HRWR dosage was adjusted by trial. By trial, adequate workability was achieved by increasing the HRWR dosage by a factor of 2. The water dosage was adjusted accordingly to account for the water content in HRWR.

Figure 4.6 IMER 360 Plus mixer used to cast a large batch of UHPC

4.5.2 Compressive Strength

Based on the findings from the previous phase of the research, it was concluded that the UHPC specimens failed prematurely from inadequate surface preparation resulting in lower strength. In the absence of an end grinder, assistance from the UDOT laboratory facility was received. However, the end grinder at the UDOT facility can only grind 4 × 8-inch (100 × 200 mm) cylinders. As such, for the strength test, three 4 × 8-inch (100 × 200 mm) cylinders were cast. This is a deviation from ASTM C1856, which specifies using only 3 × 6-inch (75 × 150 mm) cylinders. The justification for using larger cylinders with same aspect ratio can be found in the literature. In published literature, Reidel et al. reported that compressive strength marginally differs for specimens with different sizes but with the same aspect ratio (Riedel et al., 2019).

Table 4.6 presents the UHPC2 mixture's compressive strength test results. The average compressive strength is 22,213 psi (153 MPa). This is higher than the qualifying compressive strength required by ACI, ASTM, and FHWA. Therefore, the optimized mixture, UHPC2, can be classified as ultra-high-performance concrete.

Table 4.6 Compressive strength test result of UHPC2

SP	L (inch)			D (inch)			Load (lbf)	f'_c (psi)	Average f'_c (psi)
1	7.75	7.76	7.77	3.96	3.98	3.99	290,661	23,427	22,213
2	7.74	7.77	7.75	4.00	4.00	4.00	286,237	22,776	
3	7.66	7.69	7.68	3.99	3.99	4.01	256,076	20,435	

4.5.3 Freeze-Thaw Durability Test

The freeze-thaw durability tests were performed on the optimized mixture according to ASTM C666 and ASTM C215 standards. The specimens were subjected to alternating freezing and thawing cycles for 300 cycles or until the dynamic modulus of elasticity deteriorated 60% of the initial dynamic modulus of elasticity. The three UHPC2 specimens were investigated, and results are presented in Figure 4.7 and Figure 4.8. The average dynamic modulus of elasticity of the specimens at cycle 0 is 49.1 GPa. The freezing and thawing cycle gradually degrades the specimens. However, at this point of the experiment, the rate of degradation was very low. After 90 cycles, the dynamic modulus of elasticity was reduced to approximately 99.13%, as shown in Figure 4.8.

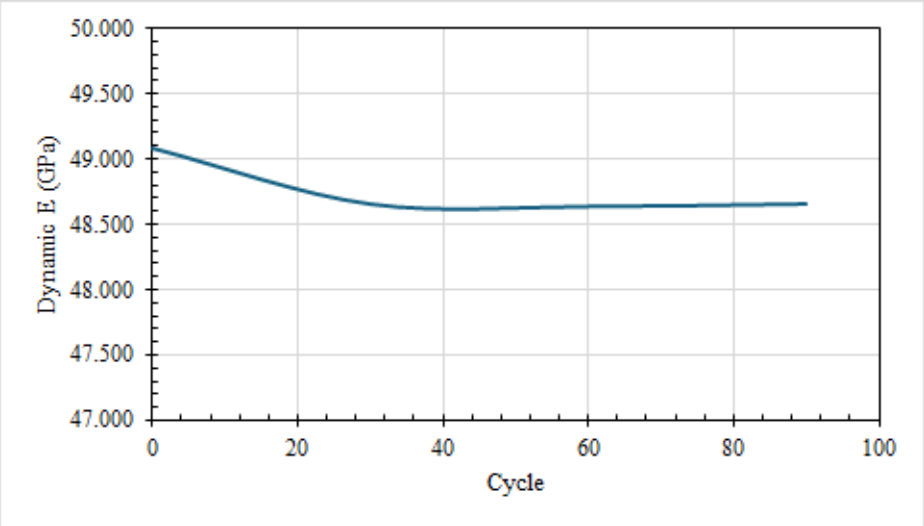

Figure 4.7 Change in dynamic modulus of elasticity under freezing-thawing condition

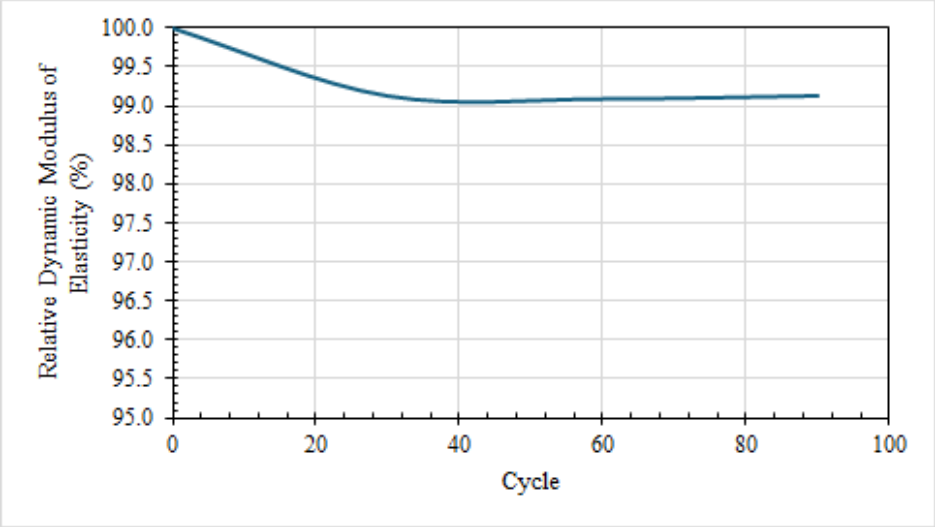

Figure 4.8 Change in relative dynamic modulus of elasticity under freezing-thawing condition

As previously noted, this test is to be conducted up to 300 cycles or until the relative dynamic modulus of elasticity (RDM) degrades below 60%. But at this stage, none of the criteria was met as the test is very lengthy and exceeds the project time period. Therefore, similar studies on RDM of UHPC mixtures with similar ingredients were studied to compare the durability of the UHPC2 specimens. The RDM of UHPC2 at 90 cycles was compared with results reported in the literature and presented in Figure 4.9. Kushzhanova et al. reported that UHPC with hybrid fibers (combination of steel and polypropylene fibers at various ratios) exhibited an increase in RDM after a freeze-thaw cycle (Kushzhanova et al., 2023). This observation was attributed to the inclusion of silica fume in the concrete mix. Silica fume reduces porosity and enhances the matrix density. Villanueva et al. evaluated the impact of different curing regimens on the durability and freeze-thaw resistance of ultra-high-strength concrete (UHSC), including fiber-reinforced variants (Muro-Villanueva et al., 2013). Depending on curing regime and presence of fiber, the RDM varied from 75% to 95%. These specimens were cured for 14 days before being subjected to a freeze-thaw cycle. Graybeal and Tanesi reported at or more than 100% RDM of UHPC specimens at 90 days, depending on how the specimens were treated (Graybeal and Tanesi, 2007). These specimens retained over 95% of their RDM after 700 cycles.

Although the number of cycles reported in this stage of the project were limited (90 cycles compared with the conventional 300), the results are promising—within the range of values reported in the literature—and indicate that UHPC2 mixture has high resistance to freeze-thaw damage. These specimens are continuously being monitored until one of the two criteria (300 cycles/60% degradation of RDM) is met.

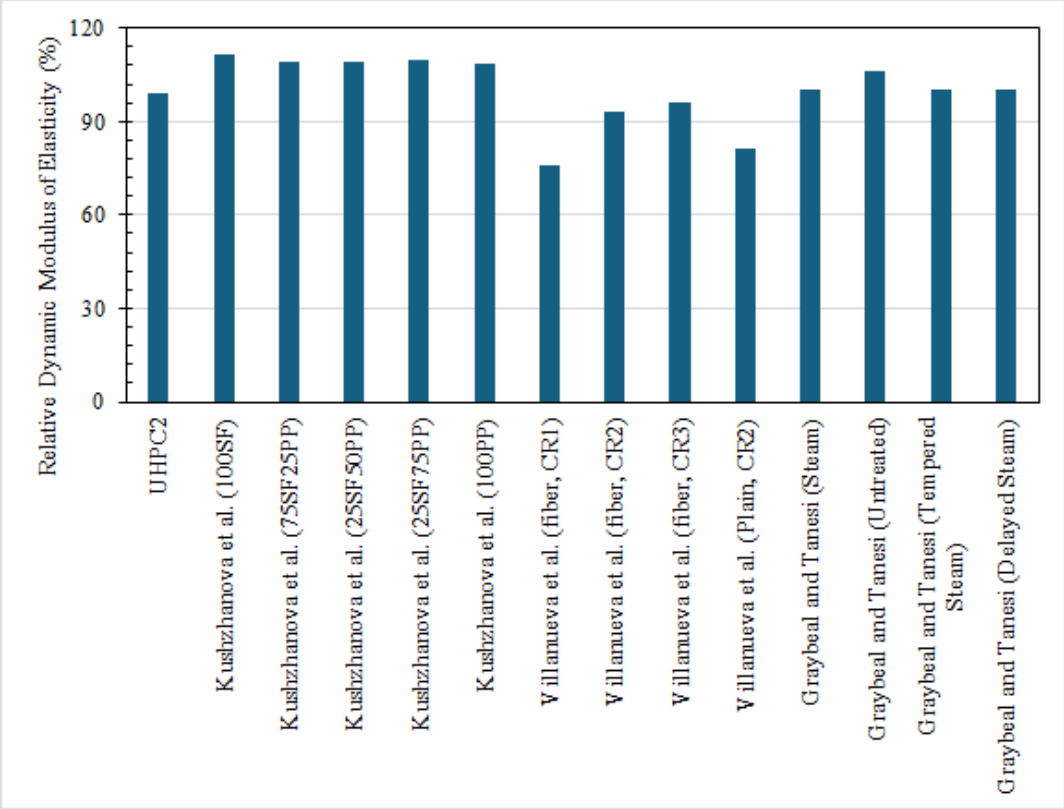

Figure 4.9 Comparison of relative dynamic modulus of elasticity at 90 cycles with the literature

4.5.4 Surface Electrical Resistivity

A surface electrical resistivity test measures a material's capability to withstand the transfer of ions subjected to an electrical field and an indicator of concrete's chloride ion penetrability. The test results are reported in Table 4.7. The average electrical resistivity ($\bar{\rho}$) is 192.58 kΩ-cm. According to the AASHTO T358, UHPC2 demonstrated very low chloride-ion penetration (Table 3.3). The dense microstructure of UHPC with a fine pore network restricts the movement of chloride ions. Thus, the risk of embedded steel reinforcement corrosion is reduced.

Table 4.7 Surface electrical resistivity test result

Batch ID	Specimen No.	$\bar{\rho}$ (kΩ-cm)				Average $\bar{\rho}$ (kΩ-cm)
UHPC2	1	197	206	203	211	192.58
	2	143	216	182	155	
	3	202	212	185	199	

The surface electrical resistivity of UHPC2 is compared with other UHPC variants with similar ingredients reported by other researchers and presented in Figure 4.10 (Sohail et al., 2021; Ghafoori, Nasiri, and Hasnat, 2022; Khaksefidi et al., 2022). The figure shows that a wide range of values for surface electrical resistivity has been reported. The average electrical resistivity of UHPC2 and the UHPC variants reported by Ghafoori et al. are between 37 and 254 kΩ-cm. This indicates very low chloride-ion penetrability. The UHPC variants reported by Sohail et al. and Khaksefidi et al. have average electrical resistivity over 254 kΩ-cm and thus have negligible chloride-ion penetrability. To summarize, the non-proprietary UHPC2 evaluated in this project demonstrates very low chloride-ion penetrability, similar to other UHPC mixes in the literature and therefore have a lower risk of embedded steel corrosion.

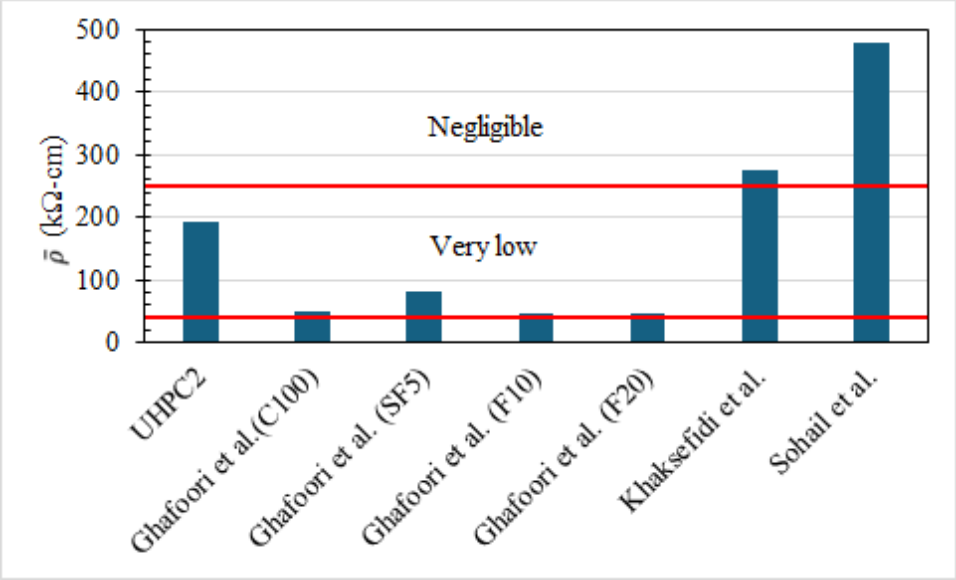

Figure 4.10 Comparison of surface electrical resistivity of UHPC with the literature

4.5.5 Drying and Autogenous Shrinkage

Drying shrinkage of the UHPC2 specimens were evaluated according to the procedure described in section 3.9 and are presented in Figure 4.11. The loss of moisture during the hardening process causes concrete to shrink. During this process, part of the available water contributes to the chemical process. Part of the excess water is expelled through bleeding. The remaining water contributes to shrinkage (Kosmatka and Wilson, 2011).

The drying shrinkage test results were reported up to 80 days after mixing. As shown in the figure, the majority of the shrinkage occurred in the initial days. At 28 days, the drying shrinkage strain was 210 microstrain. It reached 300 microstrain. at around 50 days. After that, shrinkage continuously took place but at a slower rate. On the 80th day, the drying shrinkage was 365 microstrain. UDOT requires that the long-term shrinkage of UHPC specimens to be below 766 microstrain. Therefore, the non-proprietary UHPC developed with Utah materials meets the long-term shrinkage requirement. As mentioned earlier, these specimens are still being continually monitored.

Figure 4.11 also compares the shrinkage strain results with other studies in the literature. This comparison was conducted to evaluate UHPC2 performance with respect to other variants published in the literature. Xie et al. reported shrinkage of plain (no fiber) UHPC with shrinkage reducing admixtures and different binder-to-sand ratios. UHPC2 developed as part of this research developed much smaller shrinkage strain compared with that reported by Xie et al. (Xie et al., 2018). Fu et al. reported the drying shrinkage strain of fiber reinforced UHPC for different fiber dosages. UHPC2 demonstrated lower drying shrinkage compared with the results they reported. However, the shrinkage specimens reported in their research did not undergo heat curing, unlike UHPC2 (Fu et al., 2022). Overall, UHPC2 and the other variants reported in Figure 4.11 meet UDOT's drying shrinkage limit.

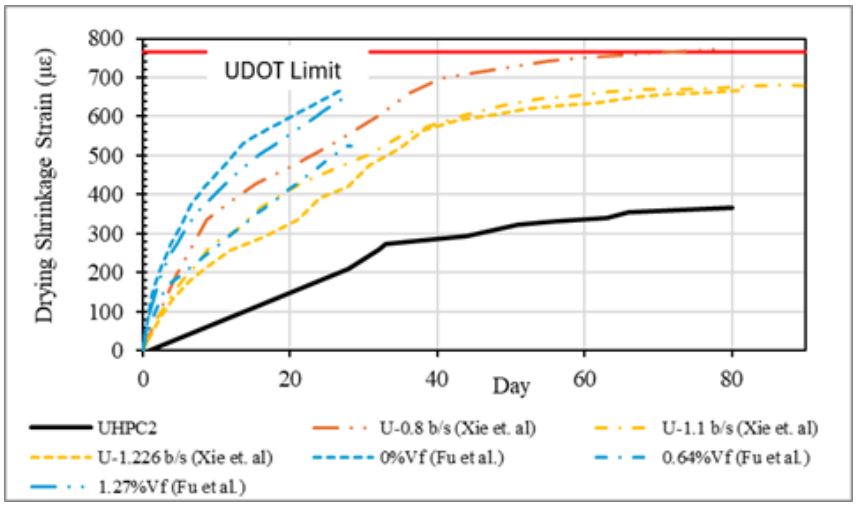

Figure 4.11 Drying shrinkage strain of UHPC2 specimens compared with shrinkage test results from the literature

Autogenous shrinkage strain of UHPC2 specimens is shown in Figure 4.12. Similar to drying shrinkage, the bulk of the autogenous shrinkage took place in the early days. Unlike the drying shrinkage specimens, autogenous shrinkage specimens were not heat cured to avoid possible melting and damage of the plastic corrugated molds used for preparing autogenous shrinkage specimens. The average autogenous shrinkage of the specimens at 28 days was 170 microstrain. Similar to drying shrinkage, the rate of shrinkage strain development decreased at later days. At 80 days, the average autogenous shrinkage strain reached 225 microstrain. UDOT does not provide a limit for autogenous shrinkage strain for locally developed UHPC.

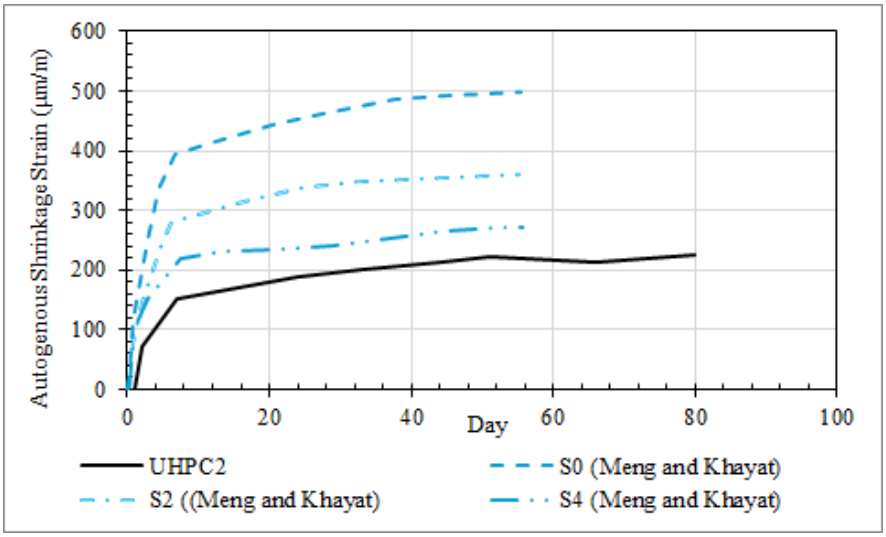

Figure 4.12 Autogenous shrinkage strain of UHPC2 specimens

Figure 4.12 also compares the autogenous shrinkage reported by Meng and Khayat for UHPC with 0%, 2%, and 4% steel fiber by volume (Meng and Khayat, 2018). UHPC2 developed in this research shows lower autogenous shrinkage compared with the shrinkage reported by Meng and Khayat. The addition and increase of fibers reduce autogenous shrinkage strain in the non-proprietary UHPC specimens.

5. CONCLUSIONS

This research program aims to develop non-proprietary UHPC mixtures using locally available materials in Utah. The following sections of this chapter present the key findings of this research program, the summary of the results, and the limitations of the findings.

5.1 Summary of Results

In this study, statistical techniques, response surface methodology along with central composite design, are employed to optimize the mixture design of a locally sourced non-proprietary UHPC mixture tailored for Utah. This statistical approach is particularly helpful when a higher number of ingredients and a wide range of their dosages are studied to optimize the mixture.

Compressive strength is the primary qualifying criterion for a cementitious composite to be classified as UHPC. The non-proprietary UHPC with locally sourced materials is optimized to obtain the characteristic strength. The final mixture design, UHPC2, meets FHWA's compressive strength requirement (17,500 psi or 120.7 MPa), ACI 239R (22,000 psi or 150 MPa), and ASTM C1856 (17,000 psi, 120 MPa). The optimum water-to-binder ratio for this mixture is 0.16, cement-to-binder ratio is 0.73, silica fume-to-binder ratio is 0.065, fly ash-to-binder ratio is 0.21, and sand-to-binder ratio is 0.7. The compressive strength of this mixture with 2% fiber by volume is 22,213 psi (153 MPa).

Freeze-thaw durability test, conducted as per ASTM C666 standard, demonstrates impressive UHPC durability performance. Dynamic modulus of elasticity was reduced to approximately 99.1% after 90 cycles, indicating low degradation rate. Another durability property, *surface resistivity*, of 192.58 kΩ-cm indicates very low chloride-ion penetration. The dense UHPC microstructure restricts chloride ion movement, reducing corrosion risk.

Drying shrinkage strain reached 210 microstrain. at 28 days, 300 microstrain. at 50 days, and 365 microstrain. at 80 days. *Autogenous shrinkage* strain was 170 microstrain. at 28 days, reaching 225 microstrain. at 80 days. UHPC meets UDOT's long-term shrinkage requirement of below 766 microstrain. These measurements highlight adequate volume stability of the developed UHPC mixture.

In conclusion, this research develops and characterizes an optimized UHPC mixture using locally sourced materials in Utah. The UHPC mixture meets durability, volume stability, and strength requirements of the local DOT. Its implementation in Utah infrastructure is expected to enhance the longevity and resilience of the state transportation systems, reducing maintenance costs and improving safety.

5.2 Recommended Future Works

While this study has demonstrated promising results in terms of freeze-thaw resistance, chloride ion penetration, and mechanical properties in the laboratory, further investigations are needed to assess the long-term performance of these mixtures under real-world conditions. Further research on exploring the long-term durability and environmental impact of UHPC mixtures developed with locally sourced, non-proprietary materials can be beneficial. Additionally, future studies can aim to optimize the use of different types of cement, alternative supplementary cementitious materials (SCMs), and fibers to enhance sustainability while maintaining or improving UHPC performance. Evaluating the life cycle cost and environmental footprint of non-proprietary UHPC compared with traditional and proprietary alternatives will also provide valuable insights for broader adoption in infrastructure projects. The application of this material as an overlay or a repair material for damaged bridge decks, columns, and beams should be investigated. Full-scale testing of the structural system cast with this new material is necessary before its widespread field application. Finally, exploring the application of advanced modeling techniques, such as machine learning, to predict UHPC behavior and optimize mixture design could lead to more efficient and tailored formulations for specific environmental conditions and structural requirements.

6. REFERENCES

AASHTO T 358 (2021) "Standard Method of Test for Surface Resistivity Indication of Concrete's Ability to Resist Chloride Ion Penetration."

ACI 239R (2018) *Ultra-High Performance Concrete: An Emerging Technology Report*.

Acker, P., and Behloul, M. (2004) "Ductal® technology: A large spectrum of properties, a wide range of applications," in Proceedings of the International Symposium on UHPC, Kassel, Germany, pp. 11–23.

AFGC (2002) *Ultra High Performance Fibre-Reinforced Concretes – Interim Recommendations*.

Ahmad, S., et al. (2019) "Mechanical properties of steel fiber-reinforced UHPC mixtures exposed to elevated temperature: Effects of exposure duration and fiber content," *Composites Part B: Engineering*, 168, pp. 291–301.

Ahmed, T., et al. (2021) "ECO-UHPC with high-volume class-F fly ash: new insight into mechanical and durability properties," *Journal of Materials in Civil Engineering*, 33(7), p. 04021174.

Akça, K.R., and Ipek, M. (2022) "Effect of different fiber combinations and optimisation of an ultra-high performance concrete (UHPC) mix applicable in structural elements," *Construction and Building Materials*, 315, p. 125777.

Alkaysi, M., et al. (2016) "Effects of silica powder and cement type on durability of ultra high performance concrete (UHPC)," *Cement and Concrete Composites*, 66, pp. 47–56.

Allena, S., and Newtson, C.M. (2011) "Ultra-high strength concrete mixtures using local materials," *Journal of Civil Engineering and Architecture*, 5(4), pp. 322–330.

Alsalman, A., et al. (2020a) "Mixture-proportioning of economical UHPC mixtures," *Journal of Building Engineering*, 27, p. 100970.

Alsalman, A., et al. (2020b) "Mixture-proportioning of economical UHPC mixtures," *Journal of Building Engineering*, 27, p. 100970.

Alsalman, A., Dang, C.N., and Hale, W.M. (2017) "Development of ultra-high performance concrete with locally available materials," *Construction and Building Materials*, 133, pp. 135–145.

Amran, M., et al. (2023) "Sustainable development of eco-friendly ultra-high performance concrete (UHPC): Cost, carbon emission, and structural ductility," *Construction and Building Materials*, 398, p. 132477.

Andrew, R.M. (2018) "Global CO 2 emissions from cement production," *Earth System Science Data*, 10(1), pp. 195–217.

Arora, A., et al. (2019) "Material design of economical ultra-high performance concrete (UHPC) and evaluation of their properties," *Cement and Concrete Composites*, 104, p. 103346.

ASTM (2017) "ASTM C1856 / C1856M - 17, Standard Practice for Fabricating and Testing Specimens of Ultra-High Performance Concrete," West Conshohocken, PA: ASTM International, pp. 1–4. Available at: https://doi.org/10.1520/C1856_C1856M-17.

ASTM C39/C39M (2018) *Standard Test Method for Compressive Strength of Cylindrical Concrete Specimens*.

ASTM C136 (2006) *Standard Test Method for Sieve Analysis of Fine and Coarse Aggregates*.

ASTM C157/C157M (2014) *Standard Test Method for Length Change Of Hardened Cement Mortar And Concrete*.

ASTM C215 (2014) *Standard Test Method for Fundamental Transverse, Longitudinal, and Torsional Resonant Frequencies of Concrete Specimens*.

ASTM C666/C666M (2015) *Standard Test Method for Resistance of Concrete to Rapid Freezing and Thawing*.

ASTM C1457 (2013) *Standard Test Method for Flow of Hydraulic Cement Mortar.*

ASTM C1698 (2019) *Standard Test Method for Autogenous Strain of Cement Paste and Mortar*.

ASTM C1856/C1856M (2017) "Standard Practice for Fabricating and Testing Specimens of Ultra-High Performance Concrete," Available at: https://doi.org/10.1520/C1856_C1856M-17.

Aydin, S. et al. (2010) "Effect of Aggregate Type on Mechanical Properties of Reactive Powder Concrete," *ACI Materials Journal*, 107(5).

Bahedh, M.A., and Jaafar, M.S. (2018) "Ultra high-performance concrete utilizing fly ash as cement replacement under autoclaving technique," *Case Studies in Construction Materials*, 9, p. e00202.

Bajaber, M.A., and Hakeem, I.Y. (2021) "UHPC evolution, development, and utilization in construction: A review," *Journal of Materials Research and Technology*, 10, pp. 1058–1074.

Banerji, S., and Kodur, V. (2022) "Effect of temperature on mechanical properties of ultra-high performance concrete," *Fire and Materials*, 46(1), pp. 287–301.

Banerji, S., Kodur, V., and Solhmirzaei, R. (2020) "Experimental behavior of ultra high performance fiber reinforced concrete beams under fire conditions," *Engineering Structures*, 208, p. 110316.

Bhanja, S., and Sengupta, B. (2005) "Influence of silica fume on the tensile strength of concrete," *Cement and Concrete Research*, 35(4), pp. 743–747.

Brühwiler, E., Denarié, E., and Habel, K. (2005) "Ultra-high performance fibre reinforced concrete for advanced rehabilitation of bridges," in Proceedings of fib-symposium, Budapest, May, pp. 23–25.

Camiletti, J., Soliman, A.M., and Nehdi, M.L. (2013) "Effect of nano-calcium carbonate on early-age properties of ultra-high-performance concrete," *Magazine of Concrete Research*, 65(5), pp. 297–307.

Central Composite Designs (CCD) (2024). Available at: https://www.itl.nist.gov/div898/handbook/pri/section3/pri3361.htm (Accessed: 17 April 2024).

Chan, Y.-W., and Chu, S.-H. (2004) "Effect of silica fume on steel fiber bond characteristics in reactive powder concrete," *Cement and Concrete Research*, 34(7), pp. 1167–1172.

Chanvillard, G., et al. (1996) “Fatigue Flexural Behaviour of Pre-Cracked Specimens of Ductal® UHPFRC,” *Lafarge*.

Chen, T., Gao, X., and Ren, M. (2018) “Effects of autoclave curing and fly ash on mechanical properties of ultra-high performance concrete,” *Construction and Building Materials*, 158, pp. 864–872.

Cheyrezy, M., Maret, V., and Frouin, L. (1995) “Microstructural analysis of RPC (reactive powder concrete),” *Cement And Concrete Research*, 25(7), pp. 1491–1500.

Collepardi, S., et al. (1997) “Mechanical properties of modified reactive powder concrete,” *ACI Special Publications*, 173, pp. 1–22.

Cui, J., et al. (2022) “Rheological properties of sprayable ultra-high performance concrete with different viscosity-enhancing agents,” *Construction and Building Materials*, 321, p. 126154.

Dehghanpour, H., et al. (2022) “Investigation of fracture mechanics, physical and dynamic properties of UHPCs containing PVA, glass and steel fibers,” *Construction and Building Materials*, 328, p. 127079.

Dils, J., Boel, V., and De Schutter, G. (2013) “Influence of cement type and mixing pressure on air content, rheology and mechanical properties of UHPC,” *Construction and Building Materials*, 41, pp. 455–463.

Dingqiang, F., et al. (2020) “A novel approach for developing a green Ultra-High Performance Concrete (UHPC) with advanced particles packing meso-structure,” *Construction and Building Materials*, 265, p. 120339.

Dong, P.S., et al. (2020) “Compressive strength development of high-volume fly ash ultra-high-performance concrete under heat curing condition with time,” *Applied Sciences*, 10(20), p. 7107.

Du, J., et al. (2021) “New development of ultra-high-performance concrete (UHPC),” *Composites Part B: Engineering*, 224, p. 109220.

El-Tawil, S., et al. (2016) *Development, Characterization and Applications of a Non Proprietary Ultra High Performance Concrete for Highway Bridges*. Michigan. Dept. of Transportation.

Feng, Y., et al. (2023) “Effects of recycled sand and nanomaterials on ultra-high performance concrete: Workability, compressive strength and microstructure,” *Construction and Building Materials*, 378, p. 131180.

Ferdosian, I., and Camões, A. (2017) “Eco-efficient ultra-high performance concrete development by means of response surface methodology,” *Cement and Concrete Composites*, 84, pp. 146–156.

FHWA (2023) *Ultra-High Performance Concrete*. Available at: https://highways.dot.gov/research/structures/ultra-high-performance-concrete/ultra-high-performance-concrete (Accessed: 1 May 2024).

fib (2010) “Model Code 2010 - First complete draft, Volume 1.”

Fu, D., et al. (2022) “Effect of concrete composition on drying shrinkage behavior of ultra-high performance concrete,” *Journal of Building Engineering*, 62, p. 105333.

Funk, J.E., and Dinger, D.R. (2013) *Predictive Process Control of Crowded Particulate Suspensions: Applied to Ceramic Manufacturing*. Springer Science & Business Media.

Ghafari, E., et al. (2015) "Influence of nano-silica addition on durability of UHPC," *Construction and Building Materials*, 94, pp. 181–188.

Ghafari, E., Costa, H., and Júlio, E. (2015) "Statistical mixture design approach for eco-efficient UHPC," *Cement and Concrete Composites*, 55, pp. 17–25.

Ghafoori, N., Nasiri, F., and Hasnat, A. (2022) "Surface resistivity for assessing the chloride transport through ultra-high-performance concrete," in *MATEC Web of Conferences*. EDP Sciences, p. 07003.

Graybeal, B., and Tanesi, J. (2007) "Durability of an ultrahigh-performance concrete," *Journal of Materials in Civil Engineering*, 19(10), pp. 848–854.

Graybeal, B.A. (2005) *Characterization of the Behavior of Ultra-High Performance Concrete*. University of Maryland, College Park.

Graybeal, B.A. (2013) *Development of Non-Proprietary Ultra-High Performance Concrete for Use In the Highway Bridge Sector: Techbrief*. United States. Federal Highway Administration.

Graybeal, B.A., and El-Helou, R. (2023) *Structural Design with Ultra-High Performance Concrete*. United States. Department of Transportation. Federal Highway Administration ….

Graybeal, B.A., and Hartmann, J.L. (2003) "Strength and durability of ultra-high performance concrete," in Concrete Bridge Conference. Portland Cement Association, Washington, DC, p. 20.

Gurusideswar, S., et al. (2020) "Tensile strength and failure of ultra-high performance concrete (UHPC) composition over a wide range of strain rates," *Construction and Building Materials*, 258, p. 119642.

Haber, Z.B., et al. (2022) *Design and Construction of UHPC-based Bridge Preservation and Repair Solutions*. United States. Federal Highway Administration. Office of Infrastructure ….

Hajar, Z., et al. (2004) "Design and construction of the world first ultra-high performance concrete road bridges," in Proceedings of the International Symposium on Ultra-High Performance Concrete, pp. 39–48.

Hamada, H., et al. (2022) "Influence of different curing methods on the compressive strength of ultra-high-performance concrete: A comprehensive review," *Case Studies in Construction Materials*, 17, p. e01390.

Hasan, T.M., Allena, S., and Gilbert, L. (2024) "Rapid chloride penetration test: An evaluation of corrosion resistance in ultra-high performance concrete," *Journal of Building Engineering*, 82, p. 108317.

Hasnat, A., and Ghafoori, N. (2021) "Freeze–thaw resistance of nonproprietary ultrahigh-performance concrete," *Journal of Cold Regions Engineering*, 35(3), p. 04021008.

He, J., et al. (2021) "The mechanical properties and damage evolution of UHPC reinforced with glass fibers and high-performance polypropylene fibers," *Materials*, 14(9), p. 2455.

Hiremath, P., and Yaragal, S.C. (2017) “Investigation on mechanical properties of reactive powder concrete under different curing regimes,” *Materials Today: Proceedings*, 4(9), pp. 9758–9762.

Le Hoang, A., and Fehling, E. (2017) “Influence of steel fiber content and aspect ratio on the uniaxial tensile and compressive behavior of ultra high performance concrete,” *Construction and Building Materials*, 153, pp. 790–806.

Huang, H. et al. (2021) “Influence of fiber alignment and length on flexural properties of UHPC,” *Construction and Building Materials*, 290, p. 122863.

Huang, W. et al. (2017) “Effect of cement substitution by limestone on the hydration and microstructural development of ultra-high performance concrete (UHPC),” *Cement and Concrete Composites*, 77, pp. 86–101.

Hung, C.-C., Chen, Y.-T., and Yen, C.-H. (2020) “Workability, fiber distribution, and mechanical properties of UHPC with hooked end steel macro-fibers,” *Construction and Building Materials*, 260, p. 119944.

Imam, A. et al. (2022) “A review study on sustainable development of ultra high-performance concrete,” *AIMS Materials Science*, 9(1), pp. 9–35.

Kalthoff, M., Raupach, M., and Matschei, T. (2021) “Influence of High Temperature Curing and Surface Humidity on the Tensile Strength of UHPC,” *Materials*, 14(15), p. 4260.

Kaptijn, N., and Blom, J. (2004) “A new bridge deck for the Kaag bridges,” *Ultra High Performance Concrete (UHPC)*, p. 49.

Khaksefidi, S., et al. (2022) “Effect of Chloride and Sulphate Environments on the Compressive Strength, Density and Electrical Resistivity of Ultra-High Performance Concrete (UHPC),” *Journal of Rehabilitation in Civil Engineering*, 10(3), pp. 158–186.

Khedr, S.A., and Abou-Zeid, M.N. (1994) “Characteristics of silica-fume concrete,” *Journal of Materials in Civil Engineering*, 6(3), pp. 357–375.

Kim, Y.J. (2018) *Development of Cost-Effective Ultra-High Performance Concrete (UHPC) for Colorado’s Sustainable Infrastructure*.

Kodur, V., Banerji, S., and Solhmirzaei, R. (2020) “Effect of temperature on thermal properties of ultrahigh-performance concrete,” *Journal of Materials in Civil Engineering*, 32(8), p. 4020210.

Kosmatka, S.H., and Wilson, M.L. (2011) *Design and Control of Concrete Mixtures*. 15th ed. Portland Cement Association.

Kushzhanova, A., et al. (2023) “Freeze-Thaw resistance and mechanical properties of UHPC reinforced with a lower amount of hybrid fibers,” *Materials Today: Proceedings* [Preprint].

Kwan, A.K.H., and Li, Y. (2013) “Effects of fly ash microsphere on rheology, adhesiveness and strength of mortar,” *Construction and Building Materials*, 42, pp. 137–145.

de Larrard, F., and Sedran, T. (1994) “Optimization of ultra-high-performance concrete by the use of a packing model,” *Cement and Concrete Research*, 24(6), pp. 997–1009.

Lawler, J.S., et al. (2019) “Development of Non-Proprietary UHPC for Florida Precast Applications,” in International Interactive Symposium on Ultra-High Performance Concrete. Iowa State University Digital Press.

Li, J., et al. (2020) “Durability of ultra-high performance concrete–A review,” *Construction and Building Materials*, 255, p. 119296.

Li, P.P., et al. (2016) “Fresh behaviour of ultra-high performance concrete (UHPC): an investigation of the effect of superplasticizers and steel fibres,” in Proceedings of the 9th International Concrete Conference 2016, Environment, Efficiency and Economic Challenges for Concrete, July 4-6, 2016, Dundee, Scotland, United Kingdom, pp. 635–644.

Li, P.P., et al. (2020) “Optimization and characterization of high-volume limestone powder in sustainable ultra-high performance concrete,” *Construction and Building Materials*, 242, p. 118112.

Li, P.P., Yu, Q.L., and Brouwers, H.J.H. (2018) “Effect of coarse basalt aggregates on the properties of Ultra-high Performance Concrete (UHPC),” *Construction and Building Materials*, 170, pp. 649–659.

Li, Z., Lu, D., and Gao, X. (2021) “Optimization of mixture proportions by statistical experimental design using response surface method-A review,” *Journal of Building Engineering*, 36, p. 102101.

Lin, Y., et al. (2019) “Effect of silica fumes on fluidity of UHPC: Experiments, influence mechanism and evaluation methods,” *Construction and Building Materials*, 210, pp. 451–460.

Liu, J., et al. (2016) “Combined effect of coarse aggregate and fiber on tensile behavior of ultra-high performance concrete,” *Construction and Building Materials*, 121, pp. 310–318.

Liu, Y., and Wei, Y. (2021) “Effect of calcined bauxite powder or aggregate on the shrinkage properties of UHPC,” *Cement and Concrete Composites*, 118, p. 103967.

Liu, Z., et al. (2018) “Effect of slag cement on the properties of ultra-high performance concrete,” *Construction and Building Materials*, 190, pp. 830–837.

Lu, Z., et al. (2021) “Freeze-thaw resistance of Ultra-High performance concrete: Dependence on concrete composition,” *Construction and Building Materials*, 293, p. 123523.

Ma, J., et al. (2004a) “Comparative investigations on ultra-high performance concrete with and without coarse aggregates,” in Proceedings of International Symposium on Ultra High Performance Concrete, Germany, pp. 205–212.

Ma, J., et al. (2004b) “Comparative investigations on ultra-high performance concrete with and without coarse aggregates,” in Proceedings of International Symposium on Ultra High Performance Concrete, Germany, pp. 205–212.

Maeder, U., et al. (2004) “Ceracem, a new high performance concrete: characterisations and applications,” in International Symposium on Ultra High Performance Concrete, (Kassel-Germany, 2004-09-13-2004-09-15), In: Schmidt M., Fehling E., Geisenhanslüke C., (eds.)*, Ultra High Performance Concrete (UHPC), Structural Materials and Engineering Series*, Kassel University, pp. 59–68.

Mazloom, M., Ramezanianpour, A.A., and Brooks, J.J. (2004) “Effect of silica fume on mechanical properties of high-strength concrete,” *Cement and Concrete Composites*, 26(4), pp. 347–357.

Meng, W., and Khayat, K.H. (2018) “Effect of hybrid fibers on fresh properties, mechanical properties, and autogenous shrinkage of cost-effective UHPC,” *Journal of Materials in Civil Engineering*, 30(4), p. 04018030.

Meng, W., Valipour, M., and Khayat, K.H. (2017) “Optimization and performance of cost-effective ultra-high performance concrete,” *Materials and Structures*, 50, pp. 1–16.

Mo, Z., Gao, X., and Su, A. (2021) “Mechanical performances and microstructures of metakaolin contained UHPC matrix under steam curing conditions,” *Construction and Building Materials*, 268, p. 121112.

Mo, Z., Wang, R., and Gao, X. (2020) “Hydration and mechanical properties of UHPC matrix containing limestone and different levels of metakaolin,” *Construction and Building Materials*, 256, p. 119454.

Montgomery, D.C. (2017) *Design and Analysis of Experiments*. John Wiley & sons.

Moore, B., and Bierwagen, D. (2006) “Ultra High Performance Concrete Design,” in HPC: Build Fast, Build to Last. The 2006 Concrete Bridge Conference Portland Cement Association. Federal Highway Administration, Nevada Department of Transportation, American Concrete Institute (ACI).

Mousavinejad, S.H.G., and Sammak, M. (2021) “Strength and chloride ion penetration resistance of ultra-high-performance fiber reinforced geopolymer concrete,” in *Structures*. Elsevier, pp. 1420–1427.

Muro-Villanueva, J., et al. (2013) “Freezing and thawing durability of ultra high strength concrete,” *Journal of Civil Engineering and Architecture*, 7(8), p. 907.

Neville, A.M. (1995) *Properties of Concrete*. Longman London.

Nguyen, T.-T., Thai, H.-T., and Ngo, T. (2021) “Optimised mix design and elastic modulus prediction of ultra-high strength concrete,” *Construction and Building Materials*, 302, p. 124150.

Nochaiya, T., Wongkeo, W.. and Chaipanich, A. (2010) “Utilization of fly ash with silica fume and properties of Portland cement–fly ash–silica fume concrete,” *Fuel*, 89(3), pp. 768–774.

Norhasri, M.S.M., *et al.* (2016) “Inclusion of nano metakaolin as additive in ultra high performance concrete (UHPC),”, *Construction and Building Materials*, 127, pp. 167–175.

Orgass, M., and Klug, Y. (2004) “Fibre reinforced ultra-high strength concretes,” in Proceedings of the International Symposium on ultra-High Performance Concrete, Kassel, Germany, pp. 637–648.

Park, S., et al. (2021) “The role of supplementary cementitious materials (SCMs) in ultra high performance concrete (UHPC): A review,” *Materials*, 14(6), p. 1472.

Patchen, A., Young, S., and Penumadu, D. (2022) “An investigation of mechanical properties of recycled carbon fiber reinforced ultra-high-performance concrete,” *Materials*, 16(1), p. 314.

Prem, P.R., Ramachandra Murthy, A., and Bharatkumar, B.H. (2015) “Influence of curing regime and steel fibres on the mechanical properties of UHPC,” *Magazine of Concrete Research*, 67(18), pp. 988–1002.

Reda, M.M., Shrive, N.G., and Gillott, J.E. (1999) “Microstructural investigation of innovative UHPC,” *Cement and Concrete Research*, 29(3), pp. 323–329.

Richard, P., and Cheyrezy, M. (1995) “Composition of reactive powder concretes,” *Cement and Concrete Research*, 25(7), pp. 1501–1511.

Richard, P., and Cheyrezy, M.H. (1994) “Reactive powder concretes with high ductility and 200-800 MPa compressive strength,” *Special Publication*, 144, pp. 507–518.

Riedel, P., et al. (2019) “Ratios of compressive strengths of ultra-high-performance concrete specimens of different shapes and sizes,” *ACI Materials Journal*, 116(6), pp. 139–149.

Rossi, P., et al. (2005) “Bending and compressive behaviours of a new cement composite,” *Cement and Concrete Research*, 35(1), pp. 27–33.

Sadrekarimi, A. (2004) “Development of a light weight reactive powder concrete,” *Journal of Advanced Concrete Technology*, 2(3), pp. 409–417.

Sadrmomtazi, A., Tajasosi, S., and Tahmouresi, B. (2018) “Effect of materials proportion on rheology and mechanical strength and microstructure of ultra-high performance concrete (UHPC),” *Construction and Building Materials*, 187, pp. 1103–1112.

Saladi, N., et al. (2023) “Assessing durability properties of ultra-high performance concrete-class materials,” *Materials and Structures*, 56(8), p. 155.

San Ha, N., et al. (2022) “Effect of grounded blast furnace slag and rice husk ash on performance of ultra-high-performance concrete (UHPC) subjected to impact loading,” *Construction and Building Materials*, 329, p. 127213.

Sarabia, L.A., Ortiz, M.C., and Sánchez, M.S. (2020) “Response surface methodology.”

Shafieifar, M., Farzad, M., and Azizinamini, A. (2017) “Experimental and numerical study on mechanical properties of Ultra High Performance Concrete (UHPC),” *Construction and Building Materials*, 156, pp. 402–411.

Shah, H.A., Yuan, Q., and Photwichai, N. (2022) “Use of materials to lower the cost of ultra-high-performance concrete–A review,” *Construction and Building Materials*, 327, p. 127045.

Shahrokhinasab, E., et al. (2021) “Effect of fiber, cement, and aggregate type on mechanical properties of UHPC,” *Civil Engineering Journal*, 7(08).

Shen, P., et al. (2019) “The effect of curing regimes on the mechanical properties, nano-mechanical properties and microstructure of ultra-high performance concrete,” *Cement and Concrete Research*, 118, pp. 1–13.

Shen, P., et al. (2020) “Investigation on expansion effect of the expansive agents in ultra-high performance concrete,” *Cement and Concrete Composites*, 105, p. 103425.

Sohail, M.G., et al. (2021) “Durability characteristics of high and ultra-high performance concretes,” *Journal of Building Engineering*, 33, p. 101669.

Soliman, A.M., and Nehdi, M.L. (2011) “Effect of drying conditions on autogenous shrinkage in ultra-high performance concrete at early-age,” *Materials and Structures*, 44, pp. 879–899.

Soliman, N.A., and Tagnit-Hamou, A. (2017) “Using Particle Packing and Statistical Approach to Optimize Eco-Efficient Ultra-High-Performance Concrete,” *ACI Materials Journal*, 114(6).

Strunge, T., and Deuse, T. (2008) “Special cements for ultra high performance concrete,” in Proceedings of the Second International Symposium on Ultra High Performance Concrete, Kassel, Germany, pp. 61–68.

Su, Y., et al. (2021) “Effect of accelerators on the workability, strength, and microstructure of ultra-high-performance concrete,” *Materials*, 15(1), p. 159.

Tafraoui, A., et al. (2009) “Metakaolin in the formulation of UHPC,” *Construction and Building Materials*, 23(2), pp. 669–674.

Teng, L., Addai-Nimoh, A., and Khayat, K.H. (2023) “Effect of lightweight sand and shrinkage reducing admixture on structural build-up and mechanical performance of UHPC,” *Journal of Building Engineering*, 68, p. 106144.

Toutanji, H.A., and Bayasi, Z. (1999) “Effect of curing procedures on properties of silica fume concrete,” *Cement and Concrete Research*, 29(4), pp. 497–501.

URMCA (2024) *UHPC – Ultra-High Performance Concrete — Another Concrete Innovation*. Available at: https://urmca.org/uhpc-ultra-high-performance-concrete-another-concrete-innovation/ (Accessed: 17 April 2024).

Wang, C., et al. (2012) “Preparation of ultra-high performance concrete with common technology and materials,” *Cement and Concrete Composites*, 34(4), pp. 538–544.

Wang, D., et al. (2015) “A review on ultra high performance concrete: Part II. Hydration, microstructure and properties,” *Construction and Building Materials*, 96, pp. 368–377.

Wang, J.N., et al. (2022) “Effect of distribution modulus (q) on the properties and microstructure development of a sustainable Ultra-High Performance Concrete (UHPC),” *Cement and Concrete Composites*, 125, p. 104335.

Wang, X., et al. (2019) “Optimized design of ultra-high performance concrete (UHPC) with a high wet packing density,” *Cement and Concrete Research*, 126, p. 105921.

Wille, K., et al. (2012) “Ultra-high performance concrete and fiber reinforced concrete: achieving strength and ductility without heat curing,” *Materials and Structures*, 45(3), pp. 309–324.

Wille, K., Naaman, A.E., and Parra-Montesinos, G.J. (2011) “Ultra-High Performance Concrete with Compressive Strength Exceeding 150 MPa (22 ksi): A Simpler Way,” *ACI Materials Journal*, 108(1).

Wong, H.H.C., and Kwan, A.K.H. (2008) “Packing density of cementitious materials: part 1—measurement using a wet packing method,” *Materials and Structures*, 41, pp. 689–701.

Wu, Z., et al. (2017) “Static and dynamic compressive properties of ultra-high performance concrete (UHPC) with hybrid steel fiber reinforcements,” *Cement and Concrete Composites*, 79, pp. 148–157.

Wu, Z., Khayat, K.H., and Shi, C. (2019) “Changes in rheology and mechanical properties of ultra-high performance concrete with silica fume content,” *Cement and Concrete Research*, 123, p. 105786.

Wu, Z., Shi, C., and Khayat, K.H. (2018) “Multi-scale investigation of microstructure, fiber pullout behavior, and mechanical properties of ultra-high performance concrete with nano-CaCO3 particles,” *Cement and Concrete Composites*, 86, pp. 255–265.

Xi, J., et al. (2022) “Role of silica fume on hydration and strength development of ultra-high performance concrete,” *Construction and Building Materials*, 338, p. 127600.

Xiao, R., Deng, Z., and Shen, C. (2014) “Properties of ultra high performance concrete containing superfine cement and without silica fume,” *Journal of Advanced Concrete Technology*, 12(2), pp. 73–81.

Xie, T., et al. (2018) “Characterizations of autogenous and drying shrinkage of ultra-high performance concrete (UHPC): An experimental study,” *Cement and Concrete Composites*, 91, pp. 156–173.

Xu, D., et al. (2023) “Influence of silica fume and thermal curing on long-term hydration, microstructure and compressive strength of ultra-high performance concrete (UHPC),” *Construction and Building Materials*, 395, p. 132370.

Xu, X., et al. (2022) “Impact properties of Ultra High Performance Concrete (UHPC) cured by steam curing and standard curing,” *Case Studies in Construction Materials*, 17, p. e01321.

Yalçınkaya, Ç., and Çopuroğlu, O. (2021) “Hydration heat, strength and microstructure characteristics of UHPC containing blast furnace slag,” *Journal of Building Engineering*, 34, p. 101915.

Yalçınkaya, Ç., and Yazıcı, H. (2017) “Effects of ambient temperature and relative humidity on early-age shrinkage of UHPC with high-volume mineral admixtures,” *Construction and Building Materials*, 144, pp. 252–259.

Yang, J., et al. (2022) “Effects of fibers on the mechanical properties of UHPC: A review,” *Journal of Traffic and Transportation Engineering (English Edition)*, 9(3), pp. 363–387.

Yang, R., et al. (2019) “Low carbon design of an Ultra-High Performance Concrete (UHPC) incorporating phosphorous slag,” *Journal of Cleaner Production*, 240, p. 118157.

Yao, J., et al. (2024) “Effects of PVA fiber on shrinkage deformation and mechanical properties of ultra-high performance concrete,” *Construction and Building Materials*, 417, p. 135399.

Yu, R., Spiesz, P., and Brouwers, H.J.H. (2014) “Effect of nano-silica on the hydration and microstructure development of Ultra-High Performance Concrete (UHPC) with a low binder amount,” *Construction and Building Materials*, 65, pp. 140–150.

Yu, R., Spiesz, P., and Brouwers, H.J.H. (2015) “Development of an eco-friendly Ultra-High Performance Concrete (UHPC) with efficient cement and mineral admixtures uses,” *Cement and Concrete Composites*, 55, pp. 383–394.

Yu, R., Spiesz, P., and Brouwers, H.J.H. (2015) “Development of Ultra-High Performance Fibre Reinforced Concrete (UHPFRC): Towards an efficient utilization of binders and fibres,” *Construction and Building Materials*, 79, pp. 273–282.

Zhang, H., et al. (2018a) “Mechanical behavior of ultra-high performance concrete (UHPC) using recycled fine aggregate cured under different conditions and the mechanism based on integrated microstructural parameters,” *Construction and Building Materials*, 192, pp. 489–507.

Zhang, H., et al. (2018b) “Mechanical behavior of ultra-high performance concrete (UHPC) using recycled fine aggregate cured under different conditions and the mechanism based on integrated microstructural parameters,” *Construction and Building Materials*, 192, pp. 489–507.

Zhou, M., et al. (2021) “Mixture design methods for ultra-high-performance concrete-a review,” *Cement and Concrete Composites*, 124, p. 104242.